

Received June 4, 2021, accepted June 20, 2021, date of publication June 28, 2021, date of current version July 7, 2021.

Digital Object Identifier 10.1109/ACCESS.2021.3093169

Novel Fuzzy-Swarm Optimization for Sizing of Hybrid Energy Systems Applying Smart Grid Concepts

ALI M. ELTAMALY^{1,2,3} AND MAJED A. ALOTAIBI^{3,4}, (Member, IEEE)

¹Sustainable Energy Technologies Center, King Saud University, Riyadh 11421, Saudi Arabia

²Electrical Engineering Department, Mansoura University, Mansoura 35516, Egypt

³Saudi Electricity Company Chair in Power System Reliability and Security, King Saud University, Riyadh 11421, Saudi Arabia

⁴Department of Electrical Engineering, College of Engineering, King Saud University, Riyadh 11421, Saudi Arabia

Corresponding author: Ali M. Eltamaly (eltamaly@ksu.edu.sa)

This work was supported by the Deanship of Scientific Research at King Saud University, Saudi Arabia, under Grant RG-1441-422.

ABSTRACT A hybrid energy system (HES) is a perfect option for supplying electric energy to remote areas. A HES normally uses renewable energy sources such as wind and PV. Owing to the intermittent nature of these sources, HES should have batteries and/or conventional energy sources. HES proposed in this study is having wind, PV, batteries, and diesel generators. The design and operation of HES are considerably improved with the use of smart grid concepts. This study introduced a fuzzy logic controller to implement a new demand response strategy (DRS) where the electricity tariff is determined based on the state of charge of the battery, the charging/discharging power from the battery, and the previous response from the customers. A modified cuckoo search (MCS) optimization algorithm is introduced for sizing HES components for the lowest cost of energy (CoE) and loss of load probability (LOLP). A multiobjective function consisting of the CoE and LOLP is used to get the optimal design of HES. The MCS reduces the number of times that the optimization algorithm executes the objective function. The continuous reduction of the swarm size proposed in this paper enhances the exploration in the beginning and enhances exploitation at the final stage. The MCS is compared with 10 state-of-the-art optimization algorithms. The results from using MCS reduced the convergence time to 25-63% of the time needed by other optimization algorithms and the DRS introduced in this study reduced the CoE by 34% compared with the flat-rate pricing.

INDEX TERMS Smart grid, hybrid energy system, fuzzy logic controller, sizing, demand response.

I. INTRODUCTION

Renewable energy sources (RES) are becoming the best option for the electricity supply of remote areas, distributed generation, as well as central power stations. The share of the worldwide generated energy from RES is about 20% [1] and it may share 50% by the end of the 21st century [2]. The intermittent nature of RES introduces reliability challenge issues to its use in the power systems. The use of batteries and diesel generators improved the performance of RES, especially in abnormal operating conditions. Different methodologies have been introduced to schedule the charging/discharging of the battery system [1], [3]. The main challenge of batteries and diesel generators is the high initial

and operating costs. For this reason, it is very important to reduce their sizes without inferior the reliability of the hybrid energy systems (HES). Modern smart grid technologies remedy the problems associated with the intermittent nature of these resources by using a demand response strategy (DRS) in which the customers can participate in the stability of HES. One of the best DRS is real-time pricing (RTP) which dynamically changes the electricity tariff based on the stability of HES. Before the recent communication revolution, the DRS was used with large loads in which the power elasticity was from -0.2 to -0.7 [3]. Another study introduced in 1999 for 40 Swiss cities estimated the price elasticity of residential load is -0.3 [4]. Another strategy estimated the price elasticity is -0.25 , -0.35 , and -0.38 for residential, commercial, and industrial customers, respectively. With the emerging smart grids, modern communication systems, and

The associate editor coordinating the review of this manuscript and approving it for publication was Resul Das ¹.

smart home applications in the modern power system, the use of active DR is becoming more feasible than before. These facilities enhance the dynamic and elasticity of the power system where the customers can receive easily the tariff on their cellular phones hourly or even part of an hour to adjust their loads based on the level of the tariff. For large micro-grid or power systems, the tariff is controlled based on the *voltage/frequency* control [5], where it can measure the stability of the power system. Meanwhile, for off-grid HES as the case introduced in this study, the tariff will be dynamically changed based on the state of charge (*SoC*) and charging/discharging power from the batteries [6].

Most of HES are using wind turbines (WTs) and PV array which need batteries and/or diesel generators to increase their stabilities during abnormal conditions. These systems sometimes used other components with the system such as fuel cells and hydrogen storage systems [7], and sometimes they used hydraulic generator systems with water tanks [8]. Also, HES sometimes works on-grid [9] or off-grid [7], [8]. The sizing of HES components has been introduced in literature without a DRS [2], [7], [10], [11] which increases the size and the cost of energy (CoE) of HES. Taking the DRS into consideration in the sizing of HES reduces the CoE and the size of its components. Most of the studies used the DRS in the operation only and overlooked its use in the sizing of HES [12]–[14], meanwhile few studies considered the DRS in the sizing stage of the system [6], [15]. Some of these studies used the DRS to determine the size of the batteries that should be connected with the existing system to improve its reliability and reduce the CoE [15]. Another study solved the sizing problem by dividing the load into high and low priority parts [16]. A recent study introduced a DRS based on a predefined formula to represent the relationship between the change in tariff with the battery *SoC* and charging/discharging power [6]. This study [6] showed an effective control to the load and substantial CoE reduction without a flexible accumulation of change in the load to be correlated with RES generation which will be solved in this study using FLC as a DRS. The FLC has been used to control the charging/discharging of residential energy systems using PV energy systems interconnected with electric utility in [13], [15], [17]. An operation of HES is introduced using FLC for optimal dispatch in [18], [19] where RES and *SoC* of the battery are introduced to FLC as an input and the output was the power dispatch for HES. The use of FLC with the grey wolf optimization (GWO) was introduced in [15] to optimally size the energy storage system by taking the energy management strategy into considerations. In this study [15], FLC is used to set the power output of the batteries, whereas, the energy management strategy is conducted based on the GWO which is used to build an adequate knowledge base for FLC [15].

Market available software such as HOMER, RETScreen, HYBRID2, HYBRIDS, HOGA, TRNSYS, HYDRO, etc. [20], have been introduced for sizing and planning of HES, but the main problem with these programs are,

they are inflexible for considering the modern smart grid strategies such as the DRS, or custom battery charging strategies, etc. [1]. For this reason, it is better to introduce flexible software to handle the planning of HES taking the smart grid concepts and other custom controllers into considerations which have been introduced effectively in this study.

Different optimization algorithms have been introduced to optimally solve the sizing problem of HES. Some of these studies introduced an iterative technique [10], or linear programming technique [21], to search for the lowest CoE from HES. The main shortcoming of these techniques is their inaccurate results where if there is a need for an accurate solution for the sizing problem the convergence time will be extraordinarily high and may be infeasible [22]. The modern soft-computing (SC) algorithms made the determining of an accurate optimal solution with reasonable convergence time is feasible and became much easier than before. Many SC algorithms have been used for solving the planning problem of HES such as genetic algorithm (GA) [14], particle swarm optimization (PSO) [23], biogeography-based optimisation (BBO) [1], artificial bee colony (ABC) [24], cuckoo search (CS) [25], bacterial foraging algorithm (BFA) [26], grasshopper optimization algorithm (GOA) [26], crow search algorithm (CSA) [8], firefly algorithm (FFA) [27], social mimic optimization (SMO) [6], grey wolf optimization (GWO) [15], and jellyfish search (JS) [28]. Some other researchers used two different SC optimization algorithms to gain the exploration performance of one SC algorithm at the beginning of the optimization and gain the exploitation performance of the other technique at the end of the optimization [1], [29]. A detailed revision of the SC algorithms used in the sizing of HES is shown in [21], [30], [31]. All these algorithms should send the values of each particle to execute the power dispatch with DRS using FLC 8760 times and then perform the cost analysis for the number of searching agents in each iteration which for sure takes a long time. This convergence time can be reduced by reducing the swarm size or by reducing the number of iterations at the expense of the accuracy of the results. The swarm size reduction decreases exploration performance, and a reduced number of iteration reduced exploitation performance which can lead to premature convergence. For this reason, it is required to reduce the convergence time without affecting the accuracy of the results and have the balance between the exploration and exploitation of the convergence which is introduced in this study. This improvement is done in this study by using a high number of swarm sizes with CS at the beginning of optimization to enhance the exploration and reduce the swarm size gradually with iteration progress to enhance the exploitation. This modified CS (MCS) algorithm introduced in this study reduced the convergence time substantially and improved the output results in terms of CoE and reliability of HES. The performance of the new proposed MCS is compared with 10 benchmark optimization algorithms to evaluate its performance. The results from this study showed that the

MCS captured the optimal solution substantially faster than the other optimization algorithms under study.

In addition to the modification introduced in this study to reduce the convergence time by MCS, a novel smart DRS is introduced in this study using FLC to solve the sizing problem based on smart grid concepts. The proposed DRS is dynamically changing the tariff to urge customers to adapt their loads to share the responsibility of HES stability between customers and HES operators. The benefit of using FLC as a DRS over the predefined methodology introduced in [6] is its independence on the knowing the exact mathematical model and the elasticity of the load from time to time. Where, the elasticity of the load is not a constant value but varies based on many factors like the time of use, the weather conditions, and the value of the required power control from the customers. The *SoC*, charging/discharging power, and the ratio between the current DR and the required change in power are used as inputs to FLC. The output from FLC is the change in tariff. The DR from the customers depends on the elasticity of the load which has a great effect on the size of RES components. The main contributions of this paper are summarized in the following points:

- Introducing a new DRS using an FLC to continually adapt the electricity tariff to ensure the stability of HES and reduces the CoE and the *LOLP*.
- Introducing MCS algorithm with gradually reducing the swarm size which substantially reduces the convergence time and the failure rate.
- Introducing the risk analysis that shows the effect of the change in data on the cost and reliability of HES.

The rest of the paper is designed to show the modeling of HES components is shown in section 2, the proposed DRS is introduced in section 3, the power dispatch of HES is introduced in section 4, the cost analysis of HES is introduced in section 5, the details of the computer program used for sizing problem is shown in section 6, the simulation results are shown in section 7, the conclusions obtained from this study are shown in section 8.

II. HYBRID ENERGY SYSTEM AVERAGE MODELING

As has been discussed in the introduction, HES has RES mainly from WTs and PV energy systems. Owing to the intermittent nature of these RES, there is a need for energy storage devices batteries, and/or diesel generators to be used as a backup for RES. The proposed HES is shown in Fig. 1 is having all these components. The PV system should be connected with the DC-bus through a DC/DC converter to control its terminal voltage to be at the voltage of the maximum power [32]. The WTs sometimes generate variable frequency which needs power electronics modifier and sometimes it generates synchronized power as the one used in this study which can be connected directly to the AC-bus as shown in Fig. 1. The batteries need a battery charger to control the operation of the battery for minimum cost and longest lifetime. The DC-bus should be connected to the AC-bus through an inverter to convert the DC power to AC.

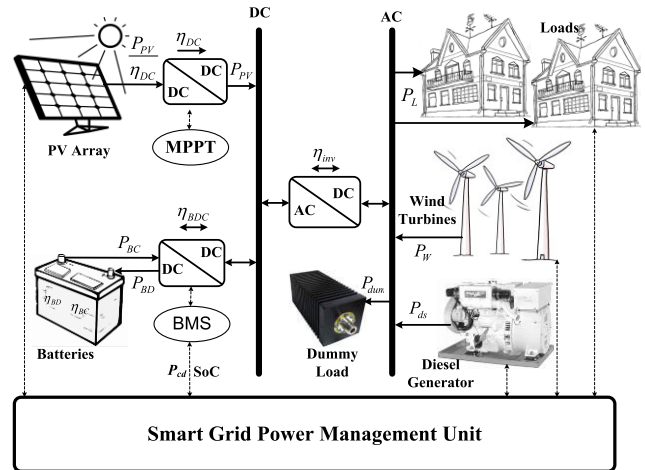


FIGURE 1. The configuration of HES.

The models of these components are introduced in the following subsections:

A. WIND ENERGY SYSTEM AVERAGE MODEL

The wind speeds are normally collected at the height of the measurement devices which may not be the same as the height of the WT and for this reason, the wind speed should be evaluated at the hub height of the WT. The relation between the wind speed at the hub height of the WT to the measurement height is shown in Eqn. (1). [33].

$$u(h) = u(h_g) * \left(\frac{h}{h_g}\right)^{1/7} \quad (1)$$

where, u is the wind speed m/s, h is the hub height of the WT, h_g is the height of the anemometer.

The generated power from the WT depends on the wind speed and the performance parameters of the WT. The generated power from the WT is shown in Eqn. (2) [33].

$$P_W(u) = \left\{ \begin{array}{ll} 0 & u \leq U_C \text{ \& } u \geq U_F \\ P_R * \frac{u^K - U_C^K}{U_R^K - U_C^K} & U_C \leq u \leq U_R \\ P_R & U_R \leq u \leq U_F \end{array} \right\} \quad (2)$$

where, U_C , U_R , and U_F are the WT cut-in, rated, and cutoff wind speeds, respectively, and K is the Weibull shape parameter of the site.

B. PV ENERGY SYSTEM MODEL

The generated power from the PV system is depending on the radiation falling on it and its terminal voltage. The maximum power point tracker (MPPT) should be used to ensure the PV array extracts the maximum available power [34]. The solar irradiances are always collected on the horizontal surface and for this reason, should be modified to the best tilt angle as introduced in [35]. The generated power from the PV array are depending on the solar irradiance, the efficiency and area of the PV array as shown in Eqn. (3) [35]. The value of the efficiency of the PV array is depending on the solar

irradiance and the temperature of the PV array as shown in Eqn. (4). The temperature of the PV array, $T_c(t)$ is a function in the temperature of the environment around it, $T_a(t)$, and the current solar irradiance as shown in Eqn. (5).

$$P_{PV}(t) = H_t(t) \cdot PVA \cdot \eta_c(t) \cdot \eta_{DC} \quad (3)$$

where, H_t is the solar radiation on an optimally tilted angle, PVA is the total area of PV array, η_{DC} is the efficiency of the DC/DC converter connected to the terminal of PV array, and $\eta_c(t)$ is the hourly efficiency of PV array which can be obtained by the following equation [33]:

$$\eta_c(t) = \eta_{cr} [1 - \beta_t \times (T_c(t) - T_{cr})] \quad (4)$$

where, β_t is the temperature coefficient and its value used in this study is 0.005 per °C [36], T_{cr} and η_{cr} are the solar cell temperature and efficiency, respectively.

$$T_c(t) = T_a(t) + 3H_t(t) \quad (5)$$

C. BATTERY STORAGE MODEL

The batteries are used to give a fast balance between the generation and the load requirements where the batteries are charged with the surplus power and discharged with the deficit power. The battery should work between the highest and lowest recommended SoC , SOC^{max} , and SOC^{min} as shown in Eqn. (6).

$$SOC^{min} < SoC(t) < SOC^{max} \quad (6)$$

where, $SOC^{min} = \frac{E_B^{min}}{E_B^{max}}$, $SOC^{max} = \frac{E_B^{max}}{E_B^{max}}$, $SoC(t) = \frac{E_B(t)}{E_B^{max}}$, E_B^{min} , and E_B^{max} are the minimum and maximum stored energy in the batteries, respectively. The rated energy of the batteries, E_B^R is usually used as a maximum allowable energy stored in the battery, $E_B^R = E_B^{max}$.

The depth of discharge (DoD) of the batteries is the difference between the SoC^{max} and SoC^{min} as shown in Eqn. (7). The usable energy from the batteries, E_{BU} in terms of DoD is shown in Eqn. (8).

$$DoD = SoC^{max} - SoC^{min} \quad (7)$$

$$E_{BU} = DoD \cdot E_B^R \quad (8)$$

The batteries are having a maximum allowable charging/discharging power, P_B^R which mainly depends on the type of battery. In most of the Lithium-ion batteries, this value is equal to $E_B^R/2$ which will be used in this study. The hourly battery power, $P_B(t)$ is the difference between the charging and discharging power and can be obtained as shown in Eqn. (9). The sign of $P_B(t)$ is positive when the generation from HES is greater than the load requirement (the battery is charging) and vice versa.

$$P_B(t) = P_{BC}(t) - P_{BD}(t) \quad (9)$$

where, $P_{BC}(t)$ and $P_{BD}(t)$ are the charging and discharging power from the battery at the DC-bus.

The batteries are losing energy every hour in case they are charging, discharging, or in case of storing conditions which

is called self-discharging. The formula showing the SoC of the batteries is shown in Eqn. (10) [37].

$$SoC(t+1) = SoC(t) \left(1 - \frac{\sigma}{24} \right) + \frac{P_{BC}(t) \cdot \eta_{BC}}{E_B^R} - \frac{P_{BD}(t)}{E_B^R \cdot \eta_{BD}} \quad (10)$$

where, σ is the self-discharge rate (SDR) which depends on the type, state of health (SoH), operating temperature, and SoC of the battery. This value is used in many studies as 0.2% per day [38], η_{BC} and η_{BD} are the charging and discharging efficiencies of the batteries, respectively.

Lithium-ion batteries work until their SoH becomes equal to 80% and it is an indication for the end of its life [17]. The aging batteries reduce the efficiency of the batteries which can be translated as a cost increase due to aging as shown in (11) [17]. This extra cost has been taken into consideration in the cost analysis section to represent the aging effects of the battery.

$$Aging\ Cost = \frac{C_B}{DoD} (1 - SoH) \quad (11)$$

where, C_B is the total cost of the batteries.

D. DIESEL GENERATOR MODEL

The proposed HES is using a diesel generator to supply the load when the generated power from RES and the batteries are inadequate to satisfy the load's need. The diesel generator is using diesel fuel to generate mechanical power to drive a synchronous generator. The diesel generator should provide at least a certain percentage of its rated power called the minimum load ratio, P_{dsr}^{min} which has been used here in this study equal to 30% of its rated power [22]. The fuel consumption of the diesel generator, $FD(l/h)$ can be obtained from Eqn.(12) [22].

$$FD(t) = B_{ds} P_{dsr} + A_{ds} P_{ds}(t) \quad (12)$$

where P_{dsr} is the rated power of the diesel generator and $P_{ds}(t)$ is the generated power at time t , B_{ds} , and A_{ds} are the fuel consumption coefficients of the diesel generator. The values of B_{ds} , and A_{ds} are chosen to be 0.08415 and 0.246, respectively [22], [39].

The efficiency of the diesel generator, η_{ds} (kWh/l) is function in its output power which can be obtained from (13) [40].

$$\eta_{ds}(t) = \frac{P_{ds}(t)}{FD(t) \cdot LHV} * 100 \quad (13)$$

where, LHV is the lower heat value of diesel fuel and its value is taken 11.55 kWh/l [40].

III. HYBRID ENERGY SYSTEM REAL-TIME MODELING

The real-time modeling of the HES is used to validate its normal operation in real-time instead of the average model is shown in section II. This model is proposed to be implemented on the Simulink. A brief discription of this model is shown in this section. The overall model of the HES in the Simulink environment is shown in Fig. 2. The same logic of

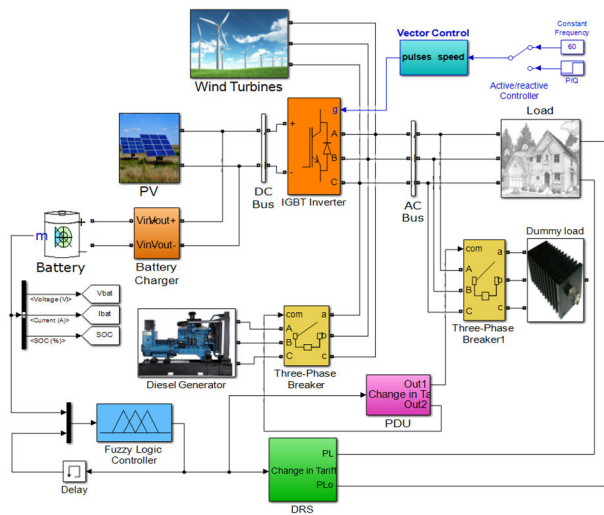


FIGURE 2. The real-time modeling of HES in Simulink.

power flow used in the average model is used here in the real-time model. A detailed discription of different parts of this model is shown in [41].

The brief discription of some models of different components in the real-time model is shown in the following subsections:

A. PV ENERGY MODEL

The PV arrays including the model of the PV modules and number of series and parallel numbers of modules, the boost converter to control the terminal voltage of the PV array, and the maximum power point tracker (MPPT) to allow the PV array to work at the maximum power point (MPP) at different irradiances and temperatures.

Different types of MPPT have been introduced in the literature [42]–[44]. The conventional MPPT algorithms like hill climbing and incremental conductance can track the MPP effectively in case of uniform distributed irradiances, meanwhile, it fails to capture the global peak in case of partial shading condition. Most of the soft computing techniques have the ability to overcome this obstacle on the expenses of convergence time. A modern optimization algorithm called musical chairs algorithm (MCA) is introduced lately which has the ability to capture the global peak in uniform irradiance and partial shading condition and it has been used in this model [42]. The idea of this proposed technique is to use a high number of search agents at the beginning of the optimization and reduces this number gradually to enhance the exploration and exploitation performance at the start and the end of the optimization steps, respectively. A detailed discription of the MCA is introduced in [42].

B. WIND ENERGY SYSTEM REAL-TIME MODELING

The real-time model of the wind turbine is shown in Fig. 4. The detailed model of this wind turbine is shown in [41]. The proposed model is designed to force the WT at its maximum

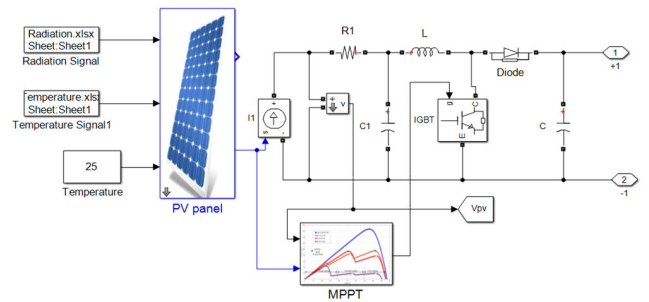


FIGURE 3. The real-time model of the PV system.

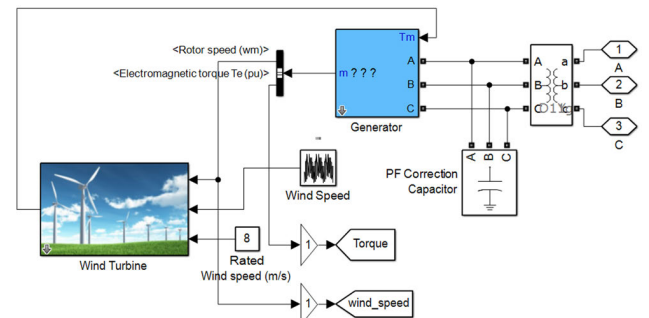


FIGURE 4. The real-time model of the wind energy system.

power point in the range of speeds below the rated speed by controlling the blades pitch angles and it forced to work at a constant power range in speeds less than the cutoff wind speeds as has been introduced in average model in Eqn. (2). Based on this control system, the model gets the current wind speed and calculates the optimal torque and rotor speed, and forces the generator to work at these values [45].

C. THE REST OF THE REAL-TIME MODEL COMPONENTS

Different components are modeled in the real-time model of the HES such as the battery which has been taken exactly as the one provided in the Simulink and the battery charger as shown in Fig. 5 [41]. The models and detailed discriptions of the DRS and the PDU are shown in the following sections.

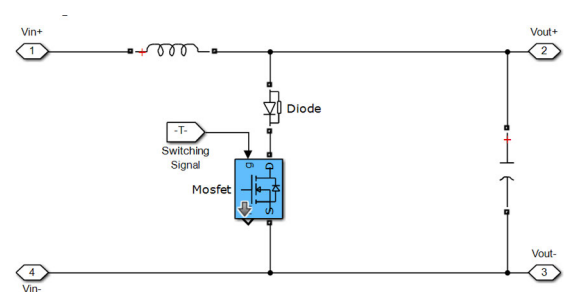


FIGURE 5. The real-time model of the battery charger.

IV. ELECTRICITY TARIFF PROGRAMS

The tariff of electricity should permit the highest benefits for the customers and investors without affecting the stability

of HES. The tariff design can encourage the customer to participate in the stability and economics of HES. Different types of tariff programs have been issued and most of these programs are falling within the categories introduced in the following subsection.

A. ELECTRICITY TARIFF CATEGORIES

The following points are showing the most tariff categories used:

1) FLAT RATE PRICING (FRP)

This tariff is using a fixed tariff all the time without taking into consideration the stability of the power system. The tariff depends on many economic and political situations of the place that are using this type of tariff [46]. This tariff may be different from one customer to another based on their monthly energy use which is sometimes called *inclining block rate (IBR)* [6]. So, the FRP is counted as an energy-based tariff. This tariff is very classic and it does not share the responsibility of the stability between the customers and the electricity providers.

2) CRITICAL PEAK PRICING (CPP)

This tariff program is using a flat tariff during the year except for few hours on few days of the year. In these periods, the tariff will be increased to force customers to reduce their demand during critical peak conditions. Sometimes, the customers positively respond to these events can get benefits and other not participant may get penalties. This tariff may be previously defined to the customers or it may be based on a call to the customer at a convenient time. This tariff may reduce the risk associated with peak periods but it will not participate in the dynamic reduction of electricity generation.

3) TIME OF USE TARIFF (TOU)

In this type of tariff the electricity suppliers provide the customer with the detailed price of electricity at the time of contract. The plan of the ToU tariff may be daily, weekly, monthly, or seasonally [6]. The energy providers issued the ToU tariff based on comprehensive studies on the load characteristics and the environmental conditions in the area. This type of tariff can be classified as power and energy-based tariff. Customers are preferring this type of tariff because they can adapt their activities based on this well-known tariff. The customers participate indirectly in the stability of the power system but it will not help in case of abnormal conditions occurred to the power system.

4) REAL-TIME PRICING (RTP)

This tariff is sometimes called the “*dynamic tariff*” in which the customers receive an announcement for the tariff one hour before where the concepts of the smart grid can be applied to monitoring the stability of the system. The *SoC* of the batteries can be used for the same purpose. RTP can effectively utilize the dynamic change in the generation from RES and reshape the loads to have a higher correlation between the

generation from RES and load which can reduce the cost of the generation and enhance the stability of the system.

B. THE NEW PROPOSED DEMAND RESPONSE STRATEGY

To encourage the customers to participate in the stability of HES, a new DRS is introduced in this study. This new DRS is using the RTP for the sizing of HES. The design of the DRS is continuously changing the tariff based on the *SoC* of the battery, the charging/discharge power to/from the batteries, and the previous response from the customers to maintain the stability of HES for all operating conditions. The novel DRS will be used in the sizing stage of HES to choose the optimal size for the lowest CoE and highest reliability. This DRS is implemented using an FLC to always adjust the load to be correlated with the available generation from RES. The logic of this novel DRS is done by using FLC to determine an hourly update for the tariff based on the stability situation of HES to urge customers to adapt their loads. Where, the tariff should be increased with low *SoC*, high discharge power, and low customer response compared with the required response and vice versa. In case the battery *SoC* is high and RES generation is higher than the load, FLC will reduce the tariff to encourage customers to increase their loads and it will keep reducing the tariff until the load is equal to the available generation for RES. On the other way, FLC will incrementally increase the tariff when the generation from RES is lower than the load until the load is equal to the available generation from RES. The level of changing the tariff is also based on the current *SoC* where the stability of HES is substantially affected by the *SoC* of the battery. This action should be continued to ensure the loads are equal to the generation from RES which can increase the stability and reduce the cost of HES. The DR from the customers is depending on the price elasticity of demand (*PED*) factor of the load. The *PED* is defined as the relation between the change in power to the change in tariff as shown in Eqn. (14). The new tariff after adding the tariff increment is shown in Eqn. (15).

$$PED = \frac{\Delta P_L(t) / P_{LA}}{\Delta \rho(t) / \rho_0} \quad (14)$$

$$\rho(t+1) = \rho(t) + \Delta \rho(t) \quad (15)$$

where, $\rho(t)$ and $\rho(t+1)$ are the tariff at the current and next hour, respectively, $\Delta \rho$ is the change in tariff, ρ_0 is the basic tariff, ΔP_L is the change in load power, P_{LA} is the average power of the original load which can be determined from Eqn. (16).

$$P_{LA} = \frac{1}{8760} \sum_{t=1}^{8760} P_{LO}(t) \quad (16)$$

where, P_{LO} is the original load power before applying the DRS.

The *PED* is normally having a negative value to represent human performance when the price of a certain commodity is increased its consumption and vice versa until the equilibrium is achieved. This logic is the same logic used in DR to control

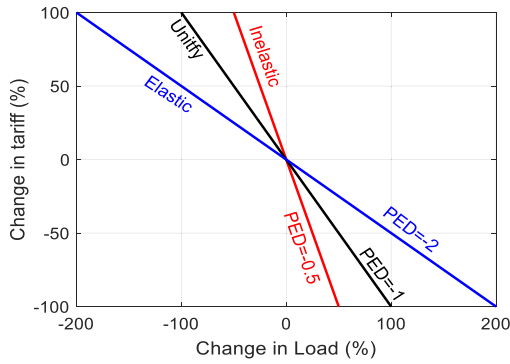


FIGURE 6. The relation between the change in price and the change in load For $PED = -0.5, -1.0, -2.0$.

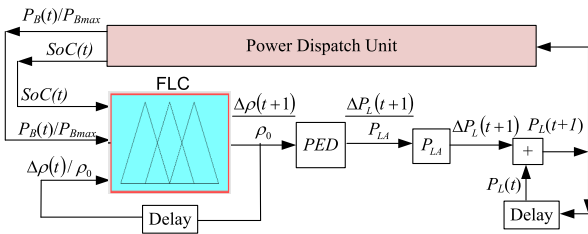


FIGURE 7. The block diagram of the demand response strategy with FLC.

the loads where the customers intend to reduce their loads when the tariff increased and vice versa. The value of PED between 0 to -1 is called inelastic loads, meanwhile, the PED between -2 to -1 is called elastic loads. When the value of $PED = -1$ the load is called unify load as shown in Fig. 6.

The proposed DRS strategy using FLC is shown in Fig. 7, where the case of the generated power from RES is lower than the load power, the deficit power will be supplied from the batteries and if it cannot feed the load the diesel generator will be used to feed this deficit power. In this case, the SoC of the batteries will keep reducing and the customers did not cooperate with the current situation the diesel engine which has a higher cost than RES will start and it may cause loss of load occurrence in case the deficit power is higher than the size of diesel generator. So, in this case, it is important to increase the tariff to urge customers to reduce/increase their loads to participate in the stability of HES. Alternatively, if the generation from RES is higher than the load power the surplus power will go to charge the battery system and if it is full, the extra power should be extracted by dummy load to maintain the stability of HES. In this case, the tariff should be reduced to encourage the customers to use the surplus energy generated from RES. So, the SoC of the battery, its power, P_B , the operation of the diesel generator, and the previous change in tariff are giving a complete picture for the situation of HES. For this reason, three variables are used as inputs to FLC which are the SoC of the battery, its power charging/discharging ratio, $P_B(t)/P_B^R$ and the current change in tariff ratio, $\Delta\rho(t)/\rho_0$ as shown in Fig. 8. The output from FLC is the new increment in tariff ratio, $\Delta\rho(t+1)/\rho_0$.

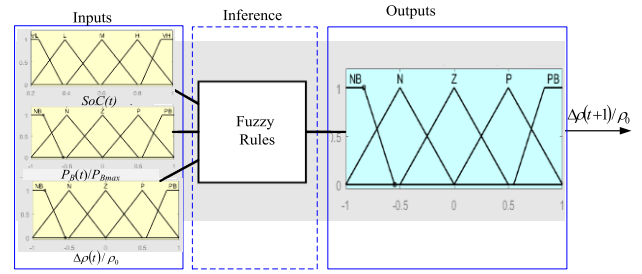


FIGURE 8. The structure of FLC.

The new increment in tariff factor, $\Delta\rho(t)/\rho_0$ will be used in the price elasticity of demand (PED) factor to determine the increment change factor in power based on the customers' response as shown in Eqn. (15). After determining the change in power, $\Delta P_L(t)$ from Eqn. (15) it will be added to the previous load power to determine the new value of load power as shown in Eqn. (17). The new value of load power will be entered to the power dispatch unit. Some studies add restrictions on the difference between the original demand load power, P_{LO} and the modified load power, P_L by $\pm 50\%$ as introduced in [12], [9].

$$P_L(t+1) = P_L(t) + \Delta P_L(t+1) \quad (17)$$

The fuzzy membership functions of the input and output variables are shown in Fig. 8. As clear from this figure that each variable has five membership functions where the SoC is having 5 five linguistic variables $VL, L, M, H,$ and VH which stand for Very Low, Low, Middle, High, and Very High, respectively. The operating range of the SoC of the battery should be set between SoC^{min} , and SoC^{max} . The other two inputs as well as the output variable from FLC are having 5 five linguistic variables $NB, N, Z, P,$ and PB which stand for Negative Big, Negative, Zero, Positive, and Positive Big, respectively. The surface functions that can represent the logic used in the rules of the FLC are shown in Fig. 10, Fig. 11, and Fig. 12.

The relation between the three inputs and the output is implemented using 125 (5^3) fuzzy rules. Fig. 9 shows a sample of the last rules of the input and output variable for random values of inputs.

V. POWER DISPATCH UNIT

The power dispatch unit (PDU) is responsible for the control of power flow between all components of HES based on its operating conditions. The power dispatch unit of HES is done based on the flowchart shown in Fig. 13 and shown in details in the steps shown in the following subsection:

A. PROPOSED DISPATCH UNIT STEPS

Step-1: Read the number of WTs, the PV array area, the batteries' size, the diesel generator size, and their other specifications. The PDU reads also the hourly wind speed, the solar radiation, the hourly load power,

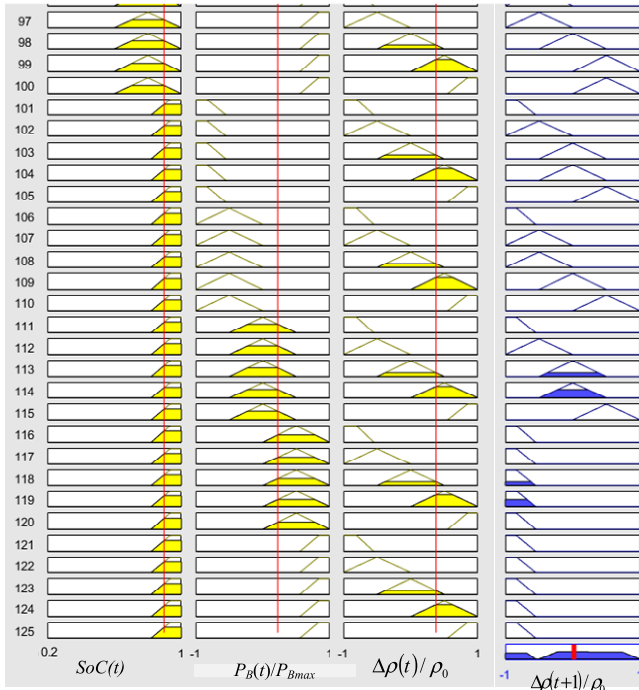


FIGURE 9. The list of the last fuzzy rules on the membership functions of the input and output variables.

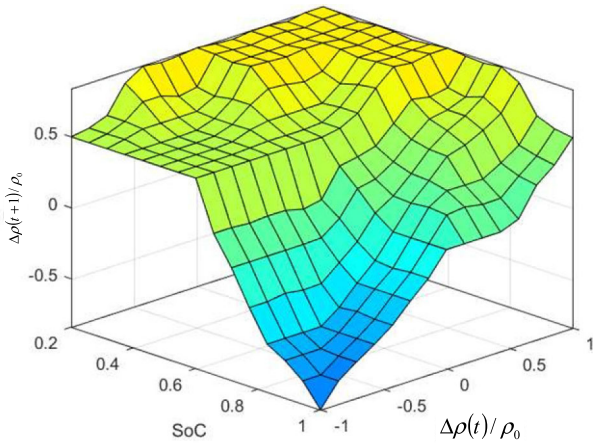


FIGURE 10. The relation between the SOC, previous change in tariff and the current change in tariff.

and set the initial increment in tariff and load power to zero.

Step-2: Determine the generated power from the WTs and PV arrays from Eqns. (2), and (3), respectively, and determine the generated power as shown in Eqn. (18).

$$P_G(t) = P_W(t) + P_{PV}(t) \cdot \eta_{inv}. \quad (18)$$

Step-3: Determine the new value of the load power, $P_L(t)$ by adding the change of power, $\Delta P_L(t+1)$ to the current load $P_L(t)$ as shown in Eqn. (17).

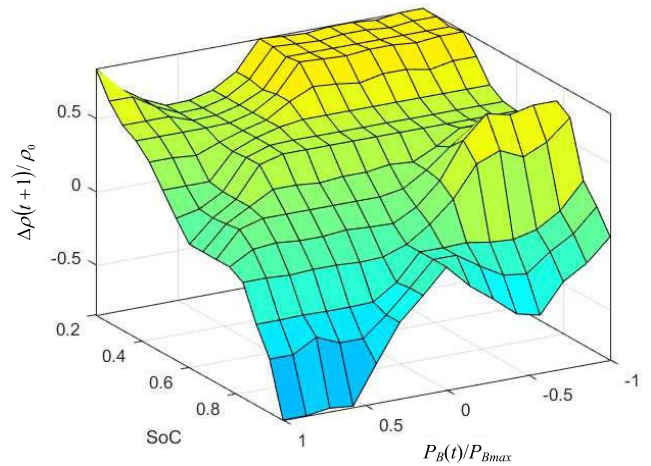


FIGURE 11. The relation between the SOC, battery power, and the current change in tariff.

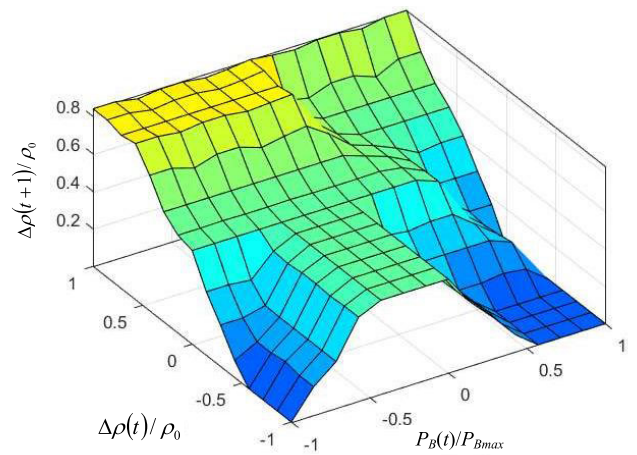


FIGURE 12. The relation between the previous change in tariff, battery power, and the current change in tariff.

Step-4: Check if $P_G(t) > P_L(t)$, go to step-5, otherwise go to step-10.

Step-5: Check if the batteries still able to charge the load ($E_B(t) < E_B^{\max}$), then go to step-6, otherwise go to step 9.

Step-6: Check if the battery can get the whole surplus power $\frac{P_G(t)-P_L(t)}{\eta_{inv} \cdot \eta_{BC} \cdot \eta_{BDC}} > E_B^{\max} - E_B(t)$, then go to step-7, otherwise go to step-8.

Step-7: Determine the battery charging power, $P_{BC}(t)$ can be obtained from Eqn. (19) and the extra power will go to the dummy load as shown in Eqn. (20) then go to step-14.

$$P_{BC}(t) = (E_B^{\max} - E_B(t)) / \eta_{BC} \quad (19)$$

$$P_{dum}(t) = P_G(t) - P_L(t) - \frac{P_{BC}(t)}{\eta_{inv}} \quad (20)$$

Step-8: The battery can extract the whole surplus power and the battery charging power will be obtained

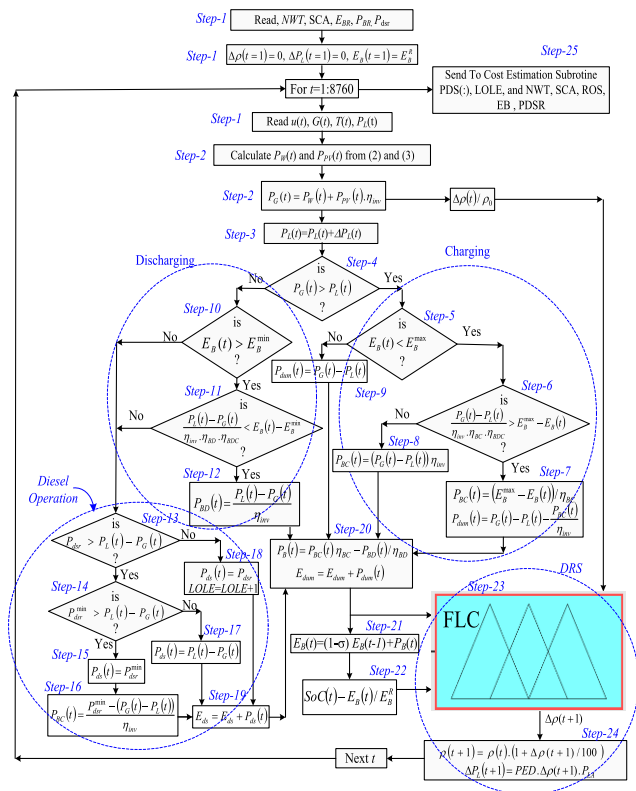


FIGURE 13. The flowchart of the power dispatch unit of HES.

from (21), then go to step-20.

$$P_{BC}(t) = P_G(t) - P_L(t) \cdot \eta_{inv} \quad (21)$$

- Step 9: As has been checked in step-5 and it is found that the battery is full, then send the surplus power to a dummy load, $P_{dum}(t) = P_G(t) - P_L(t)$ and go to step-20.
- Step-10: As has been checked in step-4, the generated power is less than the load power, $P_G(t) < P_L(t)$ which means that there is a deficit power and it should be covered by the battery or the diesel generator in case the battery cannot give the load with its need. Check if $E_B(t) > E_B^{\min}$, then go to step-11, otherwise go to step-13.
- Step-11: Check if the battery can cover the deficit power, $\frac{P_L(t) - P_G(t)}{\eta_{inv} \cdot \eta_{BD} \cdot \eta_{BDC}} < E_B(t) - E_B^{\min}$, then go to step-12, otherwise go to step-13.
- Step-12: Determine the discharging power from the battery, $P_{BD}(t) = \frac{P_L(t) - P_G(t)}{\eta_{inv} \cdot \eta_{BDC}}$ and go to step-20.
- Step-13: Check if the diesel generator can feed the deficit power, $P_{dsr} > P_L(t) - P_G(t)$, then go to step-14, otherwise go to step-18.
- Step-14: Check if the minimum diesel power is greater than the deficit power, $P_{dsr}^{\min} > P_L(t) - P_G(t)$ then got step-15, otherwise go to step 17.
- Step-15: Set the diesel power to its minimum $P_{ds}(t) = P_{dsr}^{\min}$ and send this result to step-18 & step-21.

Step-16: The extra power generated from the minimum diesel power should be sent to the battery using Eqn. (22), then go to step-19.

$$P_{BC}(t) = \frac{P_{dsr}^{\min} - (P_G(t) - P_L(t))}{\eta_{inv} \cdot \eta_{BDC}} \quad (22)$$

Step-17: If the deficit power is between the limits of the diesel generator as stated in step-13 and step-14, the diesel power can be equated to the deficit power, $P_{ds}(t) = P_L(t) - P_G(t)$, then go to step-19.

Step-18: If the deficit power is greater than the diesel maximum power, then set the diesel power to its rated value $P_{ds}(t) = P_{dsr}$ and increase the LOLP by one.

Step-19: Accumulate the diesel power $P_{ds}(t)$ to the energy from the diesel power E_{ds} , $E_{ds} = E_{ds} + P_{ds}(t)$.

Step-20: The battery energy change $P_B(t)$ can be determined from Eqn. (23) and the dummy accumulated energy can be determined from Eqn. (24). Send these values to step-21 and step-23.

$$P_B(t) = P_{BC}(t) \eta_{BC} - P_{BD}(t) / \eta_{BD} \quad (23)$$

$$E_{dum} = E_{dum} + P_{dum}(t) \quad (24)$$

Step-21: determine the current stored energy in the battery as shown in Eqn. (25) taking the self-discharge rate (σ) and charging/discharging power of the battery obtained from Eqn. (25).

$$E_B(t) = (1 - \sigma) \cdot E_B(t - 1) + P_B(t) \quad (25)$$

Step-22: Determine the SoC of the battery by dividing the current stored energy over the rated energy as shown in Eqn. (26) and send this result to FLC in step-23.

$$SoC(t) = E_B(t) / E_B^R \quad (26)$$

Step-23: Send the SoC obtained from step-22, the battery charging/discharging power ratio $P_B(t) / P_{BR}$ obtained from step-20, and the previous change in tariff $\Delta \rho(t) / \rho_0$ to FLC shown in Fig. 8 and collect the new change in tariff ratio, $\Delta \rho(t + 1) / \rho_0$.

Step-24: Determine the new value of tariff as shown in Eqn. (27) and the new change in power from Eqn. (28), Check if $t < 8760$, go to step-1, otherwise go to step-25.

$$\rho(t+1) = \rho(t) \cdot (1 + \Delta \rho(t+1)/100) \quad (27)$$

$$\Delta P_L(t+1) = PED \cdot \Delta \rho(t+1) \cdot P_{LA} \quad (28)$$

Step-25: Send the total generated energy from Eqn. (29), LOLP, E_{ds} to the cost estimation unit.

$$E_T = \sum_{t=1}^{8760} P_L(t) \quad (29)$$

B. ASSESSMENT FACTORS

Many useful factors can be extracted from the PDU which can assess the performance of HES under different operating conditions. These factors are used to evaluate the reliability, economic, and environmental performance of HES. Some of these factors are shown in the following points and some other factors are shown in literatures [6], [13], [23], [26], [47]–[53]:

C. RENEWABLE ENERGY FRACTION (REF)

This factor is representing the ratio of the generated energy from RES to the total energy supplied to the load that can be obtained from Eqn. (30) [47]–[49]. The greater the value of REF the greener HES. This factor is also called sometimes the renewable fraction [50]. To know the fraction used in the generation of wind and PV compared with the total generation from RES, two other fractions called fractions wind energy fraction (WEF) and PV energy fraction (PVEF) as shown in Eqns. (31) and (32), respectively.

$$REF = 1 - \sum_{t=1}^{8760} P_{ds}(t) / \sum_{t=1}^{8760} P_L(t) \quad (30)$$

$$WEF = \sum_{t=1}^{8760} P_W(t) / \sum_{t=1}^{8760} P_L(t) \quad (31)$$

$$PVEF = \sum_{t=1}^{8760} P_{PV}(t) / \sum_{t=1}^{8760} P_L(t) \quad (32)$$

1) CURTAILMENT LOSSES *cl*

Owing to the curtailment of the load some of the energy gets lost in the dummy load. The ratio of the lost energy in the dummy loads to the total demand load energy during the day is called the curtailment losses *l* which can be determined from (33) [48].

$$cl = \sum_{t=1}^{8760} P_{dum}(t) / \sum_{t=1}^{8760} P_L(t) \quad (33)$$

2) POWER REDUCTION RATIO K_{PR}

This factor is used to measure the ratio between the peak value of new load after using the DRS and the peak of the original load which can be obtained from Eqn. (34). The smaller the K_{PR} the effectiveness of the DRS [13].

$$K_{PR} = \max(P_L(1 : 8760)) / \max(P_{LO}(1 : 8760)) \quad (34)$$

3) PEAK TO AVERAGE POWER RATIO (PAR)

This ratio is used to measure the relationship between the peak to average power as shown in Eqn. (35), where its minimum value is 1 and the load is ideal when PAR near to 1.0 [26].

$$PAR = \frac{\max(P_L)}{\text{mean}(P_L)} \quad (35)$$

4) SUFFICIENT RATIO (SR)

This factor is used to measure the sufficient of customers from energy when they adapt their loads based on the DRS. This factor is defined as the ratio of the adapted energy from the load to the original energy required by the load as shown in Eqn. (36). The value of SR was lower than 1 means that the customers are not satisfied with the energy due to the high tariff and they are satisfied when the value of the SR is equal to or greater than 1.

$$SR = \sum_{t=1}^{8760} P_L(t) / \sum_{t=1}^{8760} P_{Lo}(t) \quad (36)$$

5) LOSS OF LOAD PROBABILITIES (LOLP)

This factor is used to measure the times that HES failed to satisfy the load's needs to the total number of hours per year (8760) as shown in Eqn. (37) [51], [52].

$$LOLP = \frac{\sum_{i=1}^{8760} t_{outage}(i)}{8760} \quad (37)$$

where, t_{outage} is representing the hour that HES failed to satisfy needs and its value is 1 or 0, where 1 is representing HES that failed to feed the load and 0 when HES satisfied the load needs.

6) LOSS OF ENERGY EXPECTED (LOEE)

LOEE is defining the ratio of the energy that HES failed to feed the load to the total energy of the load as shown in Eqn. (38) [6], [23], [53].

$$LOEE = \frac{\sum_{i=1}^{8760} P_{de}(i)}{\sum_{i=1}^{8760} P_L(i)} \quad (38)$$

where, $P_{de}(t)$ is the amount of energy that HES failed to feed the load with.

VI. ECONOMIC ANALYSIS OF THE HYBRID ENERGY SYSTEMS

The cost of the generated energy from HES is the key issue to predict its feasibility. Different cost determination strategies have been introduced in the literature to optimally size HES based on it [6], [35]. The import cost factors are shown in the following points:

A. NET PRESENT VALUE (NPV)

The NPV is a factor used to measure the feasibility of installing HES. This factor is representing the difference between the total income during the lifetime of HES and the total cost of HES through its lifetime discounted at the start of the project and can be obtained as shown in Eqn. (39). This factor is used to represent the current value of the project, the negative value of the NPV means this project should be

rejected and the acceptance of the project based on how much its positive value.

$$NPV = PVI - PVC \quad (39)$$

where, PVI is the present value of expected income, PVC is the present value of invested cash or costs. The PVI is the present value of the total income during the lifetime of the project including the income from selling salvage components during replacement and at the end of the project. The PVI of HES is shown in (40). This value of salvage of different components is shown in (41).

$$PVI = \rho \sum_{\tau=1}^T \frac{E_T * (1 - SDR)^\tau}{(1 + r)^\tau} + PSV \quad (40)$$

where, ρ is the electricity tariff, E_T is the yearly energy, SDR is the system degradation rate, PSV is the present value of salvage of components.

$$PSV = \sum_{i=1}^n \sum_{j=1}^{N_{rep}+1} \frac{SV(i)}{(1 + r)^{T*j/(N_{rep}+1)}} \quad (41)$$

where, n is the number of components that will be replaced during the lifetime of the project, N_{rep} is the number of replacements over the system life period T which can be obtained from Eqn. (42). As an example, if the project lifetime, T is 20 years, and the component i lifetime, $LT(i)$ is 6 years, then based on equation (42) the components will be replaced 3 times at year 6, 12, and, 18 which means that there are three salvage prices in the middle of the project and one at the end.

$$N_{rep} = INT (T/LT(i) - 0.01) \quad (42)$$

The PVC is the present value of the total cost of HES and any cash spent during the lifetime of the project. Moreover, the PVC is including any fixed or variable operating and maintenance cost of the whole system (OMC) as shown in Eqn. (43).

$$PVC = CC + PRC + POMC \quad (43)$$

where CC is the capital cost of the whole system including the installation cost, PRC is the present value of replacement cost, and $POMC$ is the present value of operation and maintenance costs.

The CC of HES systems including the price of all parts of the system, the installation cost, etc. which can be calculated as shown in Eqn. (44).

$$CC = WEp + PVp + BAp + DGp + SGp \quad (44)$$

where, WEp is the price of wind energy system including installation and other components needed for wind energy system, PVp is the total price of PV energy system including the installation, civil work, etc. BAp is the total price of the battery system and battery charger. DGp is the total price of the diesel generator. SGp is the total price required for

smart grid which has been used as 5% of the cost of the other components [6].

The present value of replacement cost, PRC of all the components of HES should be calculated from Eqn. (45) [37]. As an example, if the total lifetime of the project is 20, and the component, i has 6 years' lifetime, then we have $N_{rep} = 3$, then we have 3 replacements at year 6, 12, and 18 that can be obtained from using Eqn. (45).

$$PRC = \sum_{i=1}^n \sum_{j=1}^{N_{rep}} \left(\frac{RC(i)}{(1 + r)^{T*j/(N_{rep}+1)}} \right) \quad (45)$$

where, RC is the current replacement cost of the components that will be replaced during the project lifetime, N_{rep} is representing the times that the component is replaced during the lifetime of the project, T , i is the order of the components, n is the total number of components that will be replaced.

The present value of OMC of all components in HES can be determined from (46) [6]:

$$POMC = \sum_{i=1}^n \sum_{t=1}^T \frac{OMC(i)}{(1 + r)^t} \quad (46)$$

B. THE LEVELIZED COST OF ENERGY (LCOE)

The $LCOE$ is the most important economic factor that can determine the breakeven of the energy generated from HES. The $LCOE$ is simply a ratio between the total present cost of HES through its life to the discounted generated energy as shown in Eqn. (47). Many studies were introduced to determine the $LCOE$ of HES [6], [35].

$$LCOE = \frac{TPV * CRF}{E_T} \quad (47)$$

where, CRF is the capital recovery factor which is shown in (48) [6], TPV is the total cost spent through the lifetime of the project which can be obtained from subtracting the discounted salvage cost from the PVC using Eqns. (43) and (41) as shown in Eqn. (49).

$$CRF = \frac{r(1 + r)^t}{(1 + r)^t - 1} \quad (48)$$

$$TPV = PVC - PSV \quad (49)$$

VII. OPTIMIZATION ALGORITHMS

The need for an optimization algorithm is to determine the optimal sizing of the components of HES for minimum cost and highest reliability. For this reason, the optimization algorithm is using a multiobjective optimization function. The objective function that is intended to be minimized is shown in Eqn. (50). This objective function is using the $LCOE$ and $LOLP$ to mutually reduce the cost and loss of load expected from the system. To give the cost a different weight than reliability, the $LCOE$ is multiplied by a weight value, M . This factor is determined based on giving the $LCOE$ the highest value without exceeding the $LOLP$ than a predefined tolerance. Many studies are introduced in the literature to

TABLE 1. The control parameters of the benchmark optimization algorithms used in this study.

No.	Technique	Control parameters
1.	PSO [23]	$\omega=0.5, c_1=c_2=2.0$
2.	BA [6]	$f_{min}=0, f_{max}=2, \omega=1.0, A_0=1.0, r_0=0.5, \alpha, \gamma$
3.	ABC [24]	$SS=25, \omega=0.4, \text{Food number}=10$
4.	CS [25]	$P_a=0.25, \beta=1.5$
5.	GOA [26]	$l=1.5 \text{ and } f=0.5$
6.	CSA [8]	Flight length (f)=2, awareness probability (AP)=0.1
7.	FFA [27]	$\alpha(\text{randomness})=0.2, \beta(\text{attractiveness})=0.20$ and (absorption co-efficient)=1.
8.	GWO [15]	$a=2 \rightarrow 0$
9.	SMO [6]	No control parameters
10.	BFA [26]	$P_{ed}=0.5, C_b=0.01, N_{im}=20$

determine the best value of M for balance between the cost and reliability [1], [6].

$$F = M * LCOE + LOLE \tag{50}$$

where, F is the objective function, $LCOE$ is the Levelized CoE, and M is the weight value to give the $LOLP$ the required weight compared with $LCOE$.

The optimization algorithm should have fast and reliable convergence to efficiently capture the optimal solution within the lowest time. The time is a very important issue because each time the optimization algorithm executes the objective function the PDU including the DRS and cost analysis will be performed for a complete year (8760 h) which takes a substantial calculating time. The confidence of the results obtained from the optimization algorithm should be high enough to capture the global minimum condition and avoids getting trapped in one of the local peaks. For this reason, 10 optimization algorithms have been selected to perform the sizing of HES where their control parameters are shown in Table 1. Due to the long convergence time, it is very important to reduce it by reducing the number of executing the objective function without affecting the accuracy of the obtained results. This can be achieved by reducing the swarm size and/or the iteration number. The reduction of swarm size will reduce the exploration performance and the reduction of the iteration number will reduce the exploitation performance of the optimization algorithm. So, it is important to look for a solution that can reduce them without affecting the exploration and exploitation of the optimization algorithms. For this purpose, MCS is introduced in this study to reduce the convergence time and to reduce the failure rate compared with well-known optimization algorithms shown in Table 1. The idea behind using the MCS is to remove the worst (highest fitness value) particle and reduce swarm size by one in each iteration. The detailed description of the MCA is shown in the following subsection. This modification reduced the time spent in the optimization compared with 10 swarm optimization algorithms used here in this study for comparison.

A. THE MODIFIED CUCKOO SEARCH STRATEGY

The selection of the CS algorithm to look for further modification is because it is found the fastest optimization algorithm

among other state-of-the-art strategies used in this study. The CS algorithm is inspired by the parasitic behavior of the reproduction process of the cuckoo bird in nature. The cuckoo bird is always searching for a suitable nest for another bird to lay his egg inside it. In the case of the host bird has the opportunity to configure this trick it will try to select the different egg and through it out from the nest or it may abandon the nest completely. This algorithm was first introduced in 2009 by Yang, X. S., and S. Deb [54]. The CS algorithm is imitating the random nature of the searching of the cuckoo bird where it uses Lévy's flight in the searching strategy to allow the algorithm to escape from local optima and enhance the global search opportunity. The original CS algorithm uses a random position for the nests (swarm) within the allowable values of each variable and determines the fitness value for each nest. Based on the values of the fitness values of searching agents the new generation modifies the positions of the particles by adding a search step to the previous position of the nests. After getting the fitness value of the initial position of nests the new generation will check the value of each nest with a random nest and if the new value is greater than the current nest then it replaces the new nest with the better nest. If the random nest is not better than the current nest, then replace the nest position by adding the new increment as shown in Eqn. (51).

$$d_{i+1}^k = d_i^k + \alpha \cdot \frac{|u|}{v^{1/\beta}} \cdot (d_{best} - d_i^k) \tag{51}$$

where, i is the generation number ($i = 1, 2, \dots, it$), k is the order of searching agent in the swarm ($k = 1, 2, \dots, SS$), SS is the swarm-size, α is the step size which can be determined based on the problems and it is recommended in many research to be $\alpha = 1$ [54], γ and v are matrices having uniform distribution and their values can be determined as shown in Eqn (52).

$$\gamma \approx N(0, \sigma_u^2) \text{ and } v \approx N(0, \sigma_v^2) \tag{52}$$

where, the variance of γ and v can be obtained from (53)

$$\sigma_\gamma = \frac{\Gamma(1 + \beta) \cdot \sin(\pi \cdot \beta / 2)}{\Gamma(\frac{1+\beta}{2}) \cdot \beta \cdot 2^{\frac{\beta-1}{2}}} \text{ and } \sigma_v = 1 \tag{53}$$

The MCS strategy introduced in this study is performed by reducing the swarm size by one in every generation (iteration) by abandoning the worst nest. The logic behind the proposed MCS algorithm is shown in the flowchart shown in Fig. 14. The use of a high number of swarm size in initialization will enhance the exploration in the beginning and with reducing the swarm size by one in each generation it will enhance the exploitation which makes this MCS algorithm is very fast and reliable compared with the other benchmark optimization algorithms. The continuous reduction in swarm size can be stopped to any number greater than or equal to 2 as shown in Fig. 14.

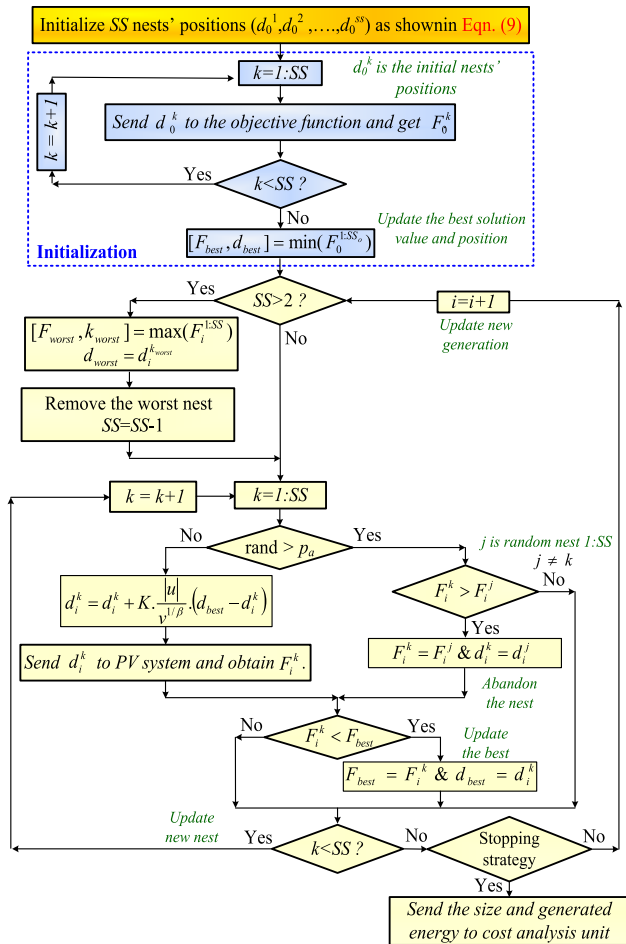


FIGURE 14. The modified cuckoo search algorithm for sizing of HES.

B. STOPPING STRATEGY

To reduce the convergence time spent to get the optimal solution a stopping strategy should be used. Many stopping strategies have been used in the literature [55], [56]. The stopping strategy used in this study is done by stopping the optimization in case the difference between the maximum and minimum values is lower than predefined tolerance as shown in Eqn. (54). In this strategy, the value of the predefined tolerance ε is used equally to 10^{-5} .

$$if \max(F(i)) - \min(F(i)) \leq \varepsilon, \text{ then } i_s = i, \text{ break} \quad (54)$$

where, i_s is the total number of iteration that the algorithm used to achieve the accuracy shown in Eqn. (54)

The number of executing the objective function is a crucial issue because the time of optimization is mainly due to getting the fitness value from the objective function wherein each time the PDU including the DRS must be executed 8760 times and the cost estimation unit also should be performed too. The number of executing the objective function, N_{SS} in all optimization algorithms under study except MCS is equal to the number of iterations times the swarm size. The number of executing the objective function in MCS is

shown in Eqn. (55).

$$N_{SS} = \begin{cases} \sum_{i=1}^{i_s} SS - (i - 1) & i_s < SS \\ SS - 1 & i_s = SS \\ \sum_{i=1}^{i_s} (SS - (i - 1)) + 2 \cdot (i_s - (SS - 1)) & i_s \geq SS \end{cases} \quad (55)$$

VIII. THE SIMULATION RESULTS

The proposed strategy and its computer program are applied to determine the optimal size for a remote site near Tabouk city in the North East of Saudi Arabia. The block diagram of the proposed software is shown in Fig. 15. The site load is selected as the load shown for a remote area near to this site and very near to the centre of the load and for this reason the transmission losses is neglected.

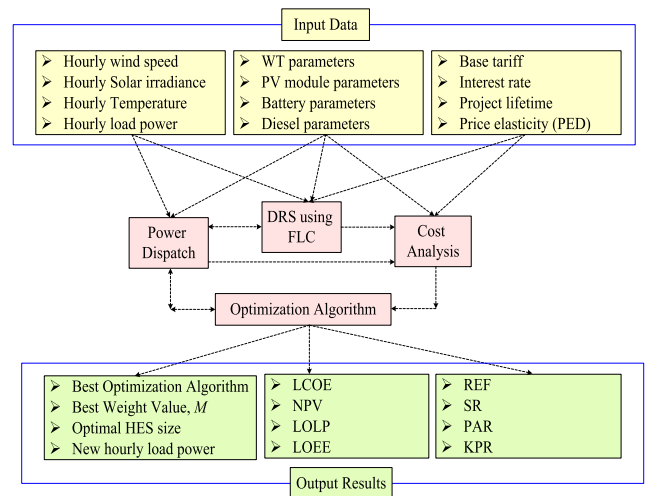


FIGURE 15. The block diagram of the new HES sizing software.

A. INPUT DATA

The input data for the proposed sizing software are listed in the following points:

- The hourly wind speed for a complete year (8760 h) at this site are shown in Fig. 16 (a). This wind speed is measured at 10 m elevation which should be updated to the hub height of the WTs (30m) using Eqn. (1).
- The hourly solar irradiance for a complete year (8760 h) for this site is shown in Fig. 16 (b) should be modified to be equal to the radiation falling on the monthly best tilt angle.
- The hourly expected load power is shown in Fig. 16 (c).
- The WTs data for selected WT called AE-Italia [57] as shown in Table. 2.
- The specifications of one of the market-available PV modules are shown in Table 3.
- The specifications of market-available battery storage are shown in Table 4.

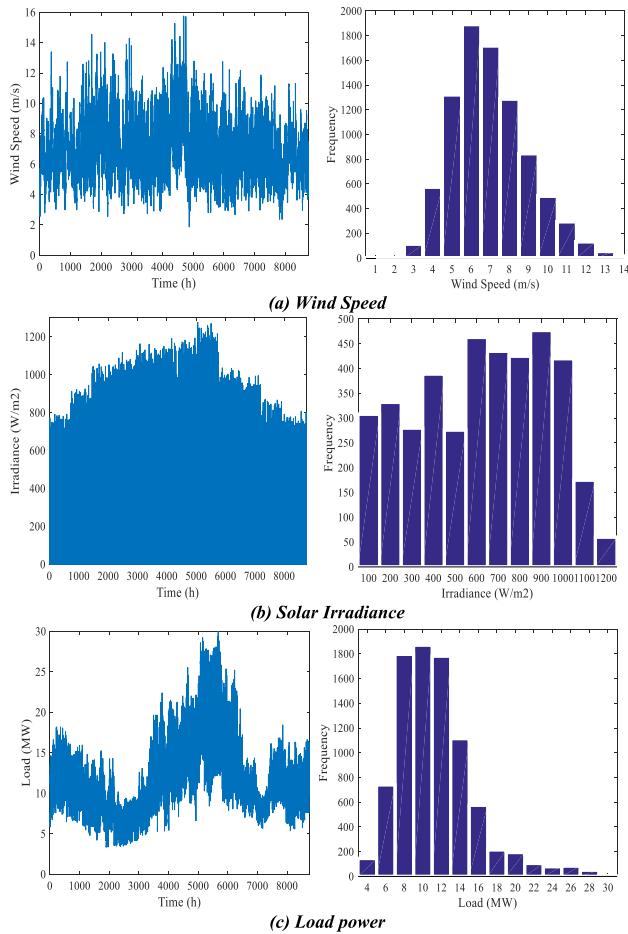


FIGURE 16. Input data (a) Wind Speed, (b) Solar Irradiance, and (c) Load power.

TABLE 2. WT parameters.

Parameter	Value used
WT cost	\$1300/kW [6]
OMC	\$100/kW/year [58]
U_C	2.5m/s [57]
U_R	8m/s [57]
U_F	25m/s [57]
WT Rated power	60 kW per WT [57]
K	2.5649
WT lifetime	20 year [25]
Hub Height	30 [57]

- The specifications of the diesel generator that may be used in this site as shown in Table 5
- The specifications of the inverter, DC/DC converter for MPPT, and battery charger as shown in Table 6

The maximum power output and input of the battery inverter related to the usable capacity is limited to 0.5 kW/kWh.

B. OUTPUT RESULTS OF THE AVERAGE MODEL

Many useful results can be extracted from this computer program. The main results are the optimal size of components for

TABLE 3. The PV specification parameters.

Parameter	Value used
PV COST	\$200/m ² [59,60]
PV OMC	0.01*PV cost [6], [61]
PV SV	25%
Area/module	1.67m ²
η_c	18%
PV lifetime	30 year
β_i	0.005 per °C
T_{cr}	25 °C
PV_{DEG}	0.5% [62]

TABLE 4. The battery specification parameters.

Parameter	Value used
Battery cost	\$250/kWh [63]
BA OMC	\$0.02/kWh/year
Battery SV	20%*BA cost
Battery life	5 years [25]
η_{BC}, η_{BD}	0.9-0.95 [64]
σ per day	0.02% [6]
DOD	80% [62]
BA_{DEG}	2 % [62]
η_{BDC}	0.95 [6]

TABLE 5. The Diesel generator specification parameters.

Parameter	Value
Cost/kW	\$250/kW [60]
Fuel cost	0.45\$/L [60]
Lifetime (operating hours)	15000 hr [60]
P_{dsr}^{min}	30% of P_{dsr} [6]

TABLE 6. The inverter specifications parameters.

Parameter	Value
Inv. cost	\$325/kW [6]
Inv. OMC	\$5/kW/year
Inv. SV	\$50/kW
T_{inv}	10 years [25], [60]
η_{inv}	0.95 [6]

the lowest cost, highest reliability, and the effect of different operating conditions on the change in this size. Some of the useful results that can be extracted from this novel program are listed in the following points:

- The hourly SoC, hourly diesel generator power, dummy load power, hourly tariff, and hourly load after application of the DRS, etc.,
- The monthly, yearly generated energy,
- The renewable generated energy ratio, and
- The convergence performance of optimization algorithms.

Three different simulation studies are introduced in this study and shown in the following subsections:

1) SELECTING THE BEST OPTIMIZATION ALGORITHM

The proposed MCS algorithm introduced in this study to improve the convergence speed of the optimization where the conversion time is an important issue due to the long-time

TABLE 7. The convergence performance of different optimization algorithms under study.

Algorithm	It	N_{SS}	t_c	t_c of MCS % of others	$LCOE$ \$/kWh	$LOLP$ (%)	F Values without units
MCS	10	205	02:33	100	0.06664	1.05836	0.077226
JS [28]	21	525	06:22	40	0.06812	1.17100	0.078815
BA [6]	13	325	04:03	63	0.06668	1.11482	0.077827
ABC [24]	17	425	05:18	48	0.06687	1.20294	0.078899
CS [25]	13	325	04:03	63	0.06719	1.12898	0.078486
GOA [26]	32	800	10:02	25	0.06711	1.10744	0.078180
CSA [8]	19	475	05:56	43	0.06700	1.17823	0.078785
FFA [27]	24	600	07:30	34	0.06733	1.16412	0.078972
GWO [15]	23	575	07:11	35	0.06701	1.16815	0.078693
SMO [6]	26	650	08:07	31	0.06677	1.19974	0.078770
BFA [26]	14	350	04:22	58	0.06706	1.18438	0.078908

consumed to execute the objective function. For this reason, it is required to reduce the times that the optimization algorithms called the objective function to determine the fitness value which is achieved by using MCS. This novel strategy reduced the swarm size by one in each generation by removing the worst agent to improve exploration at the beginning of optimization and the exploitation at the end. This proposed strategy has been compared with 10 benchmark optimization algorithms shown in Table 1. A fair evaluation of all the operating conditions for the 11 optimization algorithms should be the same. Where the swarm size for all is started with 25 particles and they will stay the same for the 10 benchmark optimization algorithms, meanwhile, it will be reduced by one in every generation for the MCS. The weight parameter, M is used in the objective function in Eqn. (50) is set to 1.0. The PED is chosen in this study to be equal to -1 . The optimization study was implemented on Matlab code using a computer having an $i7$ processor with 3.6 GHz frequency, and 20 MB cash. The results from all optimization algorithms are shown in Table 7. It is clear from this table that the fastest benchmark optimization algorithms were the traditional BA and CS with 13 iterations before the optimizations get their optimal solution which means that they called the objective function, $N_{SS} 13 \times 25 = 325$ times with about 4 hours to perform this optimization. Meanwhile, the slowest one was the GAO, where it takes 32 iterations to get the optimal conditions which means that the GAO called the objective function $32 \times 25 = 800$ times which needs more than 10 hours to perform one run of this optimization. This shows the importance of reducing the optimization time which can be achieved using the new proposed MCS algorithm. The MCS spent 10 iterations to get the optimal size of HES which means that it called the objective function 205 times based on Eqn. (55) with 2.5 h convergence time. The convergence progress of the 11 optimization algorithms used in this study is shown in Fig. 17. The results obtained from Table 7 and Fig. 17 showed that the MCS is taking from 25% to 63% of the time used for the benchmark optimization algorithms. This figure showed that the MCS is converged very fast after executing the objective function with 200 times, meanwhile, some other techniques like GOA

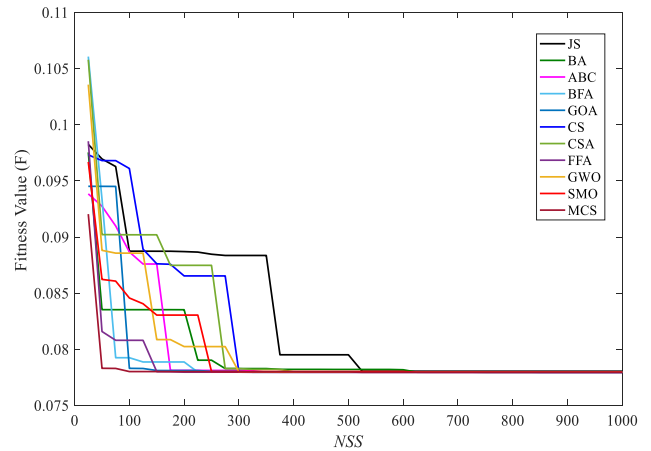


FIGURE 17. The variation of the minimum value of the minimum fitness values along with the number of executing the PDU.

executed the objective function 800 times to get the optimal solution. Moreover, the MCS is having the minimum value of fitness value, $LCOE$, and $LOLP$ compared with other benchmark optimization algorithms shown in Table 7. These results showed that MCS is superior compared with the other optimization algorithms used in this study. For this reason, MCS is the only optimization algorithm that will be used in the next simulation studies. The objective function shown in Table 7 is dimensionless because it comprises the cost and the LOLE as shown in Eqn. (50). The percent of the time consumed by MCS with respect to other optimization technique is determined by dividing the time consumed by the MCS to the time consumed by the other optimization algorithm as an example, the time consumed by the MCS compared to the time consumed by the JS is $2:33/6:22=40\%$.

2) SELECTING THE BEST VALUE OF WEIGHT

The previous study showed superior performance of MCS compared with the other optimization algorithms and for this reason, it will be used in this study. The PED used in this study is set to -1 . Variable values of weight M and the relation between the optimal fitness value, $LCOE$, and $LOLP$ are drawn as shown in Fig. 18. It is clear from this figure that increasing the value of M is reducing the $LCOE$ and increasing the $LOLP$ until the value of M has a value around 6, after that the $LCOE$ will be saturated meanwhile the value of $LOLP$ keeps increasing. So, it is not recommended to use the value of M greater than 6 because there is no reduction in cost meanwhile the $LOLP$ will be increased. The value of M can be chosen based on the desired $LOLP$, which means that if it must have $LOLP$ less than 1%, then we should choose $M = 1.0$ or lower where the cost will be $\$0.06664/kWh$. Meanwhile, if it is acceptable to have $LOLP = 5\%$, $M = 2.0$ can be chosen, and the $LCOE = 0.058$ $\$/kWh$. This means that, the cost reduction is based on expenses of reliability of HES. For this reason, the restriction of $LOLP$ will be lower than 1% and the value of $M = 1.0$ in the coming studies.

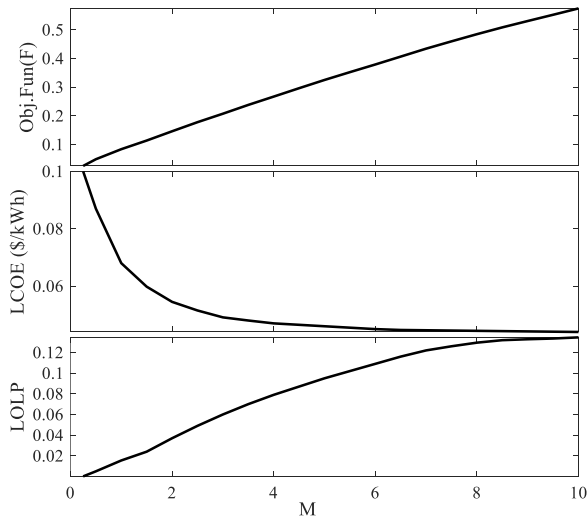


FIGURE 18. The variation of the objective function, LCOE, and LOLP with weight parameter M .

3) EFFECT OF LOAD ELASTICITY ON THE COST AND RELIABILITY OF HES

This study is very important to show the effect of demand elasticity on the sizing of HES. The sizing problem taking the DRS into account is considerably imitating the real-life when the real-time tariff is used in the smart grid system. The cost and reliability are considerably changing with the level of the elasticity of the load. The elastic load gives HES the ability to pass the critical conditions without a need for increasing the size of HES components that can reduce the cost of HES significantly. On the other way, if the load is inelastic, which means that the customers do not cooperate with the change in tariff or the FRP is used, HES should increase the size of components to be able to pass abnormal operating conditions that increase the cost of the system. This concept is discussed in this section where the relationship between the $LCOE$ and the $LOLP$ along with PED is shown in Fig. 19. It is clear from this figure that the $LCOE$ is reducing with increasing the elasticity of the load. This means that taking DRS into account can reduce the size and $LCOE$ of HES considerably which proves the importance of using smart grid concepts in the design of modern HES into consideration. It is also clear from Fig. 19 that all the performance of the HES are improved as discussed in the following points:

- The $LCOE$ is reducing from $PED = 0$ to -1 and after that, it will be saturated. The $LCOE$ is reduced from 0.073 \$/kWh with $PED = 0$ to 0.064 \$/kWh when the $PED = -2$. which means that the use of DRS will reduce the $LCOE$ by $(0.073-0.064)/0.064 = 14.1\%$.
- The $LOLP$ is reduced from 10.1% when $PED = 0$ to 1% when the $PED = -1$.
- The curtailment loss c_l which measures the energy to the dummy load till the total load energy is reduced from 30% at $PED = 0$ to 3.5% when the $PED = -1$ which means that most of the energy that was lost in the dummy

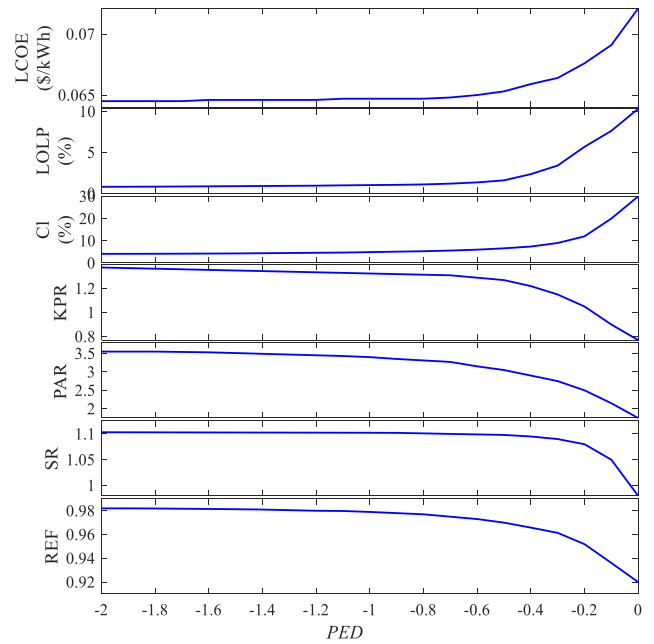


FIGURE 19. The variation of the assessment factor with along with PED .

load is used as a useful load with reduced tariff for customers.

- The power reduction ratio KPR which measures the percentage of the peak of the new load and peak of the original load is considerably improved from 0.82 at $PED = 0$ is increased to 1.28 which means that the new load power peak is improved even more than the load needs.
- The peak to average ratio, PAR is increased from 2.27 to 3.51 for $PED = 0$ and -1 , respectively, which means that HES becomes able to feed the loads with a peak greater than 3.5 of its average value.
- The SR which measures energy consumed by the new load energy to the required energy by the loads. At $PED = 0$, $SR = 0.985$ which means some of the loads cannot be supplied from HES. Once $PED = -1$, SR is increased to 1.12 which means that the load received more energy with DRS 10% than its original needs.
- The renewable energy fraction, REF which measures the contribution of RES in the load energy is increased from 0.92 without the DRS ($PED = 0$) to 0.98 when the DRS is used with $PED = -1$, which means that with the same size of the system the contribution from diesel generator is reduced from 8% to 2% of the load requirements which reduces the $LCOE$ significantly and makes HES more green.

Many studies conclude that PED is in the range of -0.4 to -0.8 and with the modern communication systems used in the smart grid this value may be increased [6]. With $PED = -1.0$ the variation of the load, generated power, battery power, SoC , diesel generator power, and dummy loads are shown in Fig. 20. This figure shows the new load power

is becoming more correlated with the generated power from RES. This achievement can be more visible when similar curves are illustrated without DRS ($PED = 0$) as shown in Fig. 21. This figure showed the big discrepancy between the load and the generated power, moreover, it showed a higher increase in diesel generator operation compared with the use of DRS ($PED = -1$). Moreover, it is clear from Fig. 17 ($PED = -1$) and Fig. 21 ($PED = 0$) that the dummy power is higher without the use of the DRS (Fig. 21) compared with the similar one when using DRS with $PED = -1$ (Fig. 20).

TABLE 8. The change in the size of HES components, diesel, and dummy energies due to the DRS.

	$PED=0$	$PED=-1$	% Change
NWT	341	285	19.6
PVA (m ²)	19,374	42,280	-54.18
E_B^R (kWh)	104,580	50,870	105.6
P_{dgr} (kW)	8,537	2,000	326.85
E_{ds} (GWh)	7.8551	2.0013	292.5
E_{dum} (GWh)	30.02	3.5023	757.15

The optimal sizes of HES components in the case of $PED = 0$ and -1 are shown in Table 8. It is clear from this table that, the use of the $PED = -1$ is reduced the size of the WT by 19.6% meanwhile it increases the PV area by -54.18% compared with the FRP ($PED = 0$). Also, it is cleared from this table that the need for batteries is increased by 105.6% when used FRP compared with $PED = -1$. Also, it is clear from Table 8 that the energy generated from the diesel generator and the energy lost in the dummy loads are increased by 292.5% and 757.15% when used FRP compared with $PED = -1$.

From the results shown in Table 8, the WT numbers, batteries, and diesel generator power is significantly reduced when using DRS with $PED = -1$ compared with the FRP ($PED = 0$), meanwhile, the PV area is increased.

4) THE RISK ANALYSIS

The risk analysis is very important to predict the change in cost and other important factors when one or more factors were not accurate enough in the data. The first study introduced in this section is in case of the wind speed is changed $\pm 20\%$. This study is conducted by changing the wind speed as shown in Fig. 22. It is clear from this figure that when the wind speed is increased by 20% the cost is dropped from 0.0657 \$/kWh to 0.0653 \$/kWh and the LOLP is reduced from 1% to 0.03%. Meanwhile, if the wind speed is reduced by -20% the LCOE is increased from 0.0657 \$/kWh to 0.0858 \$/kWh and the LOLP will be increased from 1% to 5.5%.

Similar study is conducted with the PV energy system as shown in Fig. 23 where the values of solar irradiances are increased by $\pm 20\%$. It is clear from this figure that in case of increase the solar irradiances by 20%, the LCOE is reduced from 0.0657 \$/kWh to 0.0642 \$/kWh and the

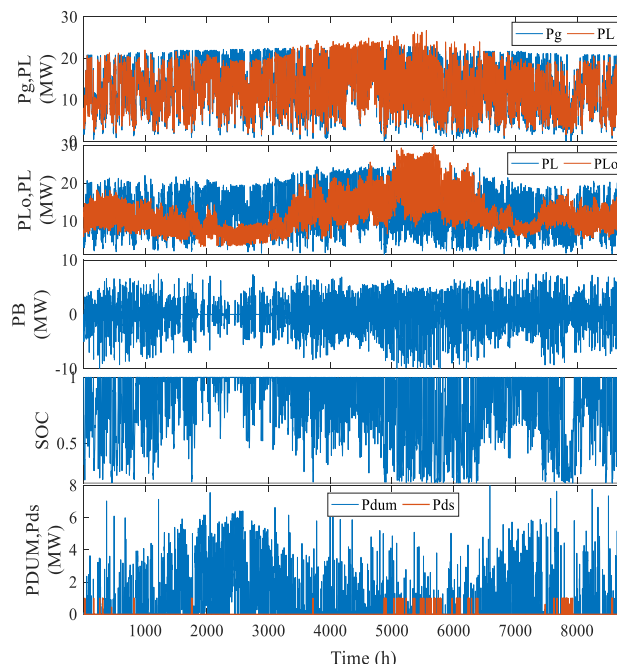


FIGURE 20. The time variation of load, generated power, diesel, and dummy powers as well as the battery power and SoC with $PED = -1$.

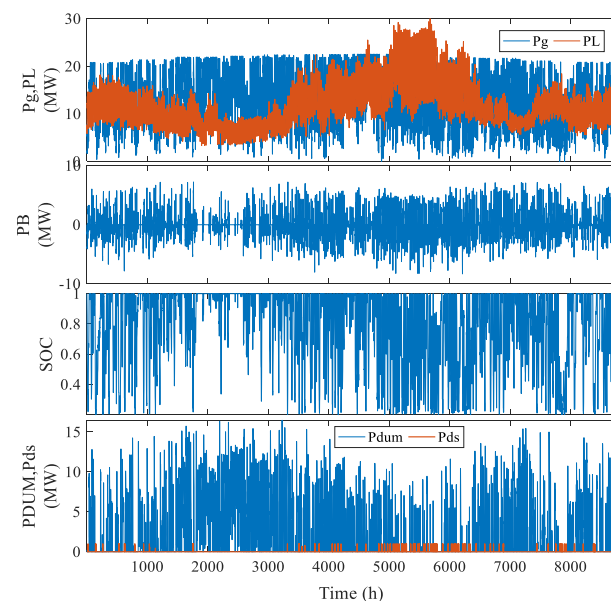


FIGURE 21. The time variation of load, generated power, diesel, and dummy powers as well as the battery power and the SoC with $PED = 0$.

LOLP is reduced from 1% to 0.07%. Meanwhile, if the solar irradiances are reduced by -20% the LCOE is increased from 0.0657 \$/kWh to 0.082 \$/kWh and the LOLP will be increased from 1% to 1.7%.

As discussed before the LCOE and LOLP have an inverse relationship where this study is introduced for different values of PED as shown in Fig. 24. This study is performed by variation of weight value, M . It is clear from this figure that

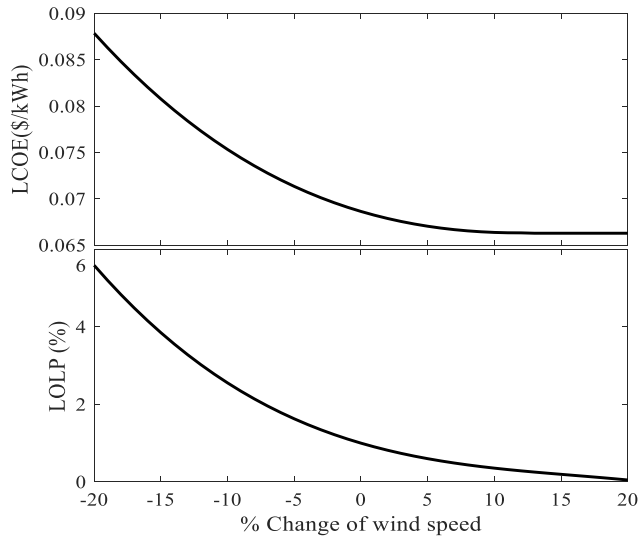


FIGURE 22. The effect of wind speed data changes on the LCOE and the LOLP.

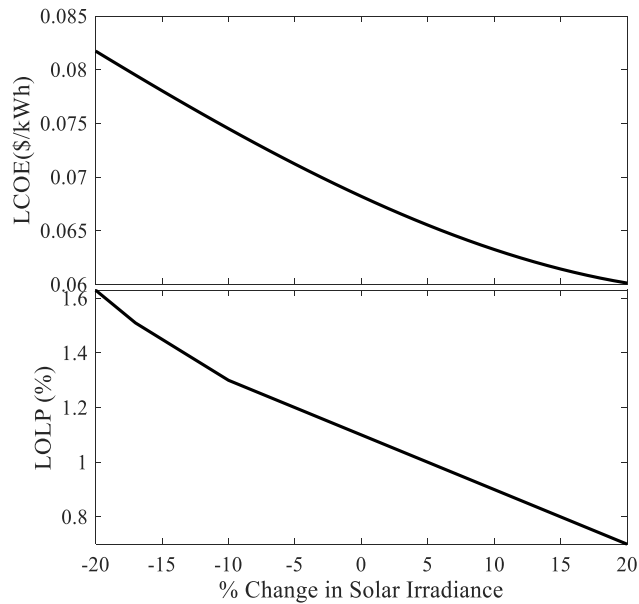


FIGURE 23. The effect of solar irradiances data changes on the LCOE and LOLP.

the PED has a great influence on the values of LCOE, and LOLP which proves the superiority of using DRS and FLC.

C. THE SIMULATION RESULTS OF THE REAL-TIME MODEL

The real-time model described in section III is implemented on the Simulink simulation program for the same results obtained from the average sizing optimization program shown in Table 8. The system is simulated for 10 s with variable wind speed, solar irradiances, load, and at starting SOC of the battery 80%. The variation of the solar irradiance (W/m²), wind speed (m/s), the generated power and load power, battery power, and SOC of the battery are shown

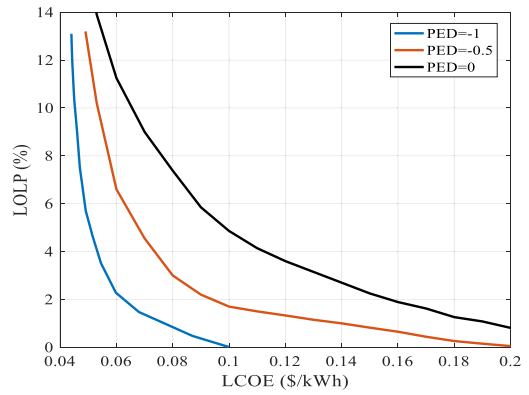


FIGURE 24. The relation between the LOLP with the LCOE for different values of elasticity.

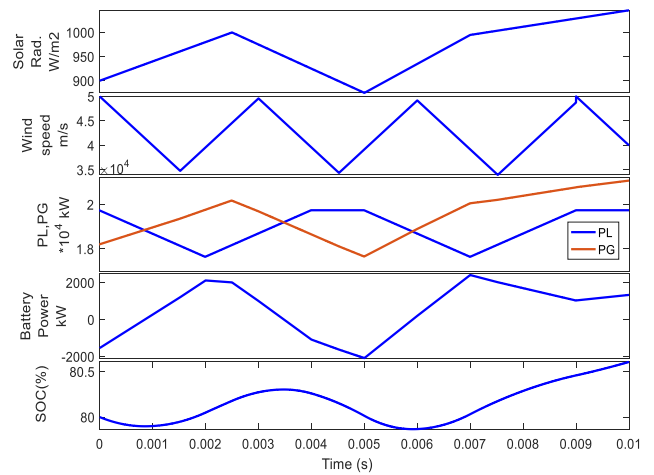


FIGURE 25. The time variation of the results of real-time model.

in Fig. 25. The results obtained from the real-time simulation model shows the superior performance of the HES system under varying weather and load variations.

IX. CONCLUSION

Hybrid energy systems (HES) are becoming attractive options for generating electricity for remote communities. Taking the demand response strategy (DRS) into considerations using real-time pricing (RTP) as one of the smart grid concepts reduces the size of HES components significantly. With a modern communication system, the need for the application of a smart grid will reduce the cost of energy (CoE) and increase system reliability where customers will participate in the stability of HES and they will benefit from reducing their electricity bills. This study proposed a demand response strategy (DRS) using a fuzzy logic controller (FLC) that varies the tariff based on the stability situation of HES. The proposed DRS is using the SoC and the charging/discharging power of the batteries as inputs to FLC and the output is the change in tariff. Based on this technique the customers will adapt their loads to avoid the high tariff periods and excess their loads in the low tariff periods. This strategy will

enhance the correlation between the load and the available generation from renewable energy sources which can significantly reduce CoE and increase reliability of HES. The use of MCS optimization algorithm reduced the convergence time by 25% to 63% compared with 10 benchmark optimization algorithms used in this study which proved the superiority of the MCS compared with the benchmark optimization algorithms in terms of the convergence time and accuracy. The results from this study showed that the required sizes for HES components are increased by 19.6%, 105.6, and 326.85% for the WTs, batteries kWh, and the diesel generator size, respectively with used flat-rate pricing (FRP) compared with the DRS with $PED = -1$, meanwhile, the size of the PV is reduced by -54.18% . More results are obtained from this study where the salient results are shown in the following points:

- The CoE and loss of load expected (LOLP) are reduced by 14.1 and 10.1%, respectively when DRS is used compared with the FRP.
- The loss of the generated energy in the dummy load is reduced from 30% to 3.5% when DRS is used compared with the FRP.
- The sufficient ratio that measures the new load energy compared with the original load is increased from 0.985 to 1.12 when DRS is used compared with the FRP.
- The renewable energy fraction, REF is increased from 0.92 to 0.98 when DRS is used compared with the FRP.
- The change in wind speed data $\pm 20\%$ will change the LCOE from 0.0653 \$/kWh to 0.0858 \$/kWh.
- The change in wind speed data $\pm 20\%$ will change the LOLP from 0.03% to 5.5%.
- The change in solar irradiance data $\pm 20\%$ will change the LCOE from 0.0642 \$/kWh to 0.082 \$/kWh.
- The change in wind speed data $\pm 20\%$ will change the LOLP from 0.07% to 1.7%.

LIST OF SYMBOLS

h	Hub height of the WT.
u	Wind speed m/s
h_g	Height of the anemometer
U_C	Cut-in wind speed
U_R	Rated wind speed of the WT
U_F	Cutoff wind speed of the WT
K	Weibull shape parameter.
P_{PV}	PV output power at the DC-bus
P_W	Wind energy system generated power
P_G	The total generated power from the wind and PV at the AC-bus
PVA	PV area (m ²)
H_t	Solar irradiance
η_c	Efficiency of PV array
η_{DC}	Efficiency of the PV DC/DC converter.
η_{cr}	Rated solar cell efficiency
T_{cr}	Rated solar cell temperature
T_c	Solar cell temperature

T_a	Ambient temperature
t	Time (h) (1:8760)
β_t	Temperature coefficient
SoC	State of charge of the batteries
DoD	Depth of discharge of the batteries
SoH	State of health of the batteries
SoC^{min}	Minimum SoC
SoC^{max}	Maximum SoC
$E_B(t)$	Hourly batteries' stored energy
E_B^{min}	minimum stored energy in the batteries
E_B^{max}	Maximum stored energy in the batteries
E_B^R	The rated energy of the batteries
P_B^R	Maximum allowable charging/discharging power
P_B	Charging/discharging batteries' power
P_{BC}	Charging batteries' power
P_{BD}	Discharging batteries' power
σ	Self-discharge rate
η_{BC}, η_{BD}	Charging/discharging efficiency of the batteries
C_B	Total cost of the batteries
$FD (l/h)$	Fuel consumption of the diesel generator
P_{dsr}	Rated power of the diesel generator
$P_{ds}(t)$	Hourly Diesel generator power
P_{dsr}	Rated power of diesel generator
E_{ds}	Total generated power from the diesel
P_{dsr}^{min}	Minimum allowable power from diesel
B_{ds}, A_{ds}	Fuel consumption coefficients of the diesel generator
η_{ds}	Diesel generator efficiency
LHV	Lower heat value of diesel fuel
$\rho(t)$	Electricity tariff
ρ_0	Basic electricity tariff
P_{LA}	Average power of the original load
P_{LO}	Original load power
P_L	Modified load power
PED	Price elasticity of demand factor
η_{inv}	Inverter efficiency
η_{BDC}	Battery charger efficiency
P_{dum}	Dummy power
E_{dum}	Total energy lost in the dummy load
E_T	Total load energy after using DRS.
E_{TO}	Total energy of the original load
REF	Renewable energy fraction
WEF	Wind energy fraction
$PVEF$	PV energy fraction
Cl	Curtailement losses
K_{PR}	Power reduction ratio
PAR	Peak to average power ratio
SR	Sufficient ratio
$LOLP$	Loss of load probabilities
$LOEE$	Loss of energy expected
P_{de}	The deficit in load power
NPV	Net present value
PVI	Present value of expected income
PVC	Present value of invested cash

OMC	operating and maintenance cost of the whole system
SDR	The system degradation rate.
r	interest or discount rate
T	Project lifetime
PSV	present value of salvage of all components
SV	Salvage value of each component
n	Number of components in HES
N_{rep}	Number of replacements over the system life period
$LT(i)$	Lifetime of component i
CC	Total capital cost
PRC	Total replacement cost
POMC	Present value of operation and maintenance costs
WEp	Price of wind energy system
PVp	Price of PV energy system
BAp	Price of the battery system
DGp	Price of the diesel generator price
SGp	Smart grid components cost
RC(i)	Replacement cost of the component i
LCOE	Levelized cost of energy
CRF	Capital recovery factor
TPV	Total cost spent
M	Weight constant of the objective function
SS	Swarm size
d_i^k	Particle position of particle k at iteration i .
α	Step length of CS particles
d_{best}	Best position of CS particles
ε	Predefined tolerance
i_s	Number of iterations to the stopping strategy
i_t	Total number of iterations in the optimization algorithms
N_{SS}	Total times the objected function executed
P_{WR}	Rated power of each WT
PV_{DEG}	Degradation factor of PV
P_{dsr}^{min}	Minimum allowable load of diesel generator

LIST OF ABBREVIATIONS

HES	Hybrid energy system
DR	Demand response
DRS	Demand response strategy
CS	Cuckoo search algorithm
MCS	Modified cuckoo search algorithm
CoE	Cost of energy
PV	Photovoltaic
RES	Renewable energy sources
RTP	Real-time pricing
SoC	State of charge
DoD	Depth of discharge
WT	Wind turbine
FLC	Fuzzy logic controller
GWO	Grey wolf optimization
GA	Genetic algorithm
SC	Soft-computing
PSO	Particle swarm optimization

BBO	Biogeography-based optimisation
ABC	Artificial bee colony
BFA	Bacterial foraging algorithm
GOA	Grasshopper optimization algorithm
CSA	Crow search algorithm
FFA	Firefly algorithm
SMO	Social mimic optimization
LOLP	Loss of load probability
MPPT	Maximum power point tracker
FRP	Flat rate pricing
IBR	Inclining block rate
CPP	Critical peak pricing
ToU	Time of use tariff
PDU	power dispatch unit

REFERENCES

- [1] A. Abuelrub, M. Khamees, J. Ababneh, and H. Al-Masri, "Hybrid energy system design using greedy particle swarm and biogeography-based optimisation," *IET Renew. Power Gener.*, vol. 14, no. 10, pp. 1657–1667, Jul. 2020.
- [2] S. Hussain, R. Al-Ammari, A. Iqbal, M. Jafar, and S. Padmanaban, "Optimisation of hybrid renewable energy system using iterative filter selection approach," *IET Renew. Power Gener.*, vol. 11, no. 11, pp. 1440–1445, Sep. 2017.
- [3] D. R. Bohi and M. B. Zimmerman, "An update on econometric studies of energy demand behavior," *Annu. Rev. Energy*, vol. 9, no. 1, pp. 105–154, Nov. 1984.
- [4] M. Filippini, "Swiss residential demand for electricity," *Appl. Econ. Lett.*, vol. 6, no. 8, pp. 533–538, Aug. 1999.
- [5] Y. Luo, L. Shi, and G. Tu, "Optimal sizing and control strategy of isolated grid with wind power and energy storage system," *Energy Convers. Manage.*, vol. 80, pp. 407–415, Apr. 2014.
- [6] A. M. Eltamaly, M. A. Alotaibi, A. I. Alolah, and M. A. Ahmed, "A novel demand response strategy for sizing of hybrid energy system with smart grid concepts," *IEEE Access*, vol. 9, pp. 20277–20294, 2021.
- [7] R. Hosseinalizadeh, H. G. Shakouri, M. S. Amalnick, and P. Taghipour, "Economic sizing of a hybrid (PV-WT-FC) renewable energy system (HRES) for stand-alone usages by an optimization-simulation model: Case study of Iran," *Renew. Sustain. Energy Rev.*, vol. 54, pp. 139–150, Feb. 2016.
- [8] S. Makhdoomi and A. Askarzadeh, "Optimizing operation of a photo-voltaic/diesel generator hybrid energy system with pumped hydro storage by a modified crow search algorithm," *J. Energy Storage*, vol. 27, Feb. 2020, Art. no. 101040.
- [9] A. Zeh and R. Witzmann, "Operational strategies for battery storage systems in low-voltage distribution grids to limit the feed-in power of roof-mounted solar power systems," *Energy Procedia*, vol. 46, pp. 114–123, Jan. 2014.
- [10] A. M. Eltamaly and M. A. Mohamed, "A novel software for design and optimization of hybrid power systems," *J. Brazilian Soc. Mech. Sci. Eng.*, vol. 38, no. 4, pp. 1299–1315, 2016.
- [11] G. Tuna, R. Das, and V. C. Gungor, "Communications technologies for smart grid applications: A review of advances and challenges," in *Smart Grid Analytics for Sustainability and Urbanization*, vol. 1, Z. H. Gontar, Ed., 1st ed. Hershey, PA, USA: IGI Global, 2018, pp. 215–235.
- [12] J. Bergner, J. Weniger, T. Tjaden, and V. Quaschnig, "Feed-in power limitation of grid-connected PV battery systems with autonomous forecast-based operation strategies," in *Proc. 29th Eur. Photovolt. Sol. Energy Conf. Exhib.*, 2014, pp. 2363–2370.
- [13] K. H. Chua, Y. S. Lim, and S. Morris, "A novel fuzzy control algorithm for reducing the peak demands using energy storage system," *Energy*, vol. 122, pp. 265–273, Mar. 2017.
- [14] J. Veras, I. Silva, P. Pinheiro, R. Rabêlo, A. Veloso, F. Borges, and J. Rodrigues, "A multi-objective demand response optimization model for scheduling loads in a home energy management system," *Sensors*, vol. 18, no. 10, p. 3207, Sep. 2018.

- [15] K. S. El-Bidairi, H. D. Nguyen, S. D. G. Jayasinghe, T. S. Mahmoud, and I. Peneis, "A hybrid energy management and battery size optimization for standalone microgrids: A case study for Flinders Island, Australia," *Energy Convers. Manage.*, vol. 175, pp. 192–212, Nov. 2018.
- [16] A. M. Eltamaly, M. A. Mohamed, M. S. Al-Saud, and A. I. Alolah, "Load management as a smart grid concept for sizing and designing of hybrid renewable energy systems," *Eng. Optim.*, vol. 49, no. 10, pp. 1813–1828, Oct. 2017.
- [17] Y.-S. Cheng, H. Hesse, N. Truong, A. Jossen, and Y.-H. Liu, "Charging strategy for a residential battery storage system using fuzzy logic controller," in *Proc. NEIS Conf.*, 2016, pp. 182–189.
- [18] A. Derrouazin, M. Aillerie, N. Mekakia-Maaza, and J.-P. Charles, "Multi input-output fuzzy logic smart controller for a residential hybrid solar-wind-storage energy system," *Energy Convers. Manage.*, vol. 148, pp. 238–250, Sep. 2017.
- [19] M. Žarković and G. Dobrić, "Fuzzy expert system for management of smart hybrid energy microgrid," *J. Renew. Sustain. Energy*, vol. 11, no. 3, May 2019, Art. no. 034101.
- [20] S. Sinha and S. S. Chandel, "Review of software tools for hybrid renewable energy systems," *Renew. Sustain. Energy Rev.*, vol. 32, pp. 192–205, Apr. 2014.
- [21] S. Sinha and S. S. Chandel, "Review of recent trends in optimization techniques for solar photovoltaic-wind based hybrid energy systems," *Renew. Sustain. Energy Rev.*, vol. 50, pp. 755–769, Oct. 2015.
- [22] Y. A. Katsigiannis, P. S. Georgilakis, and E. S. Karapidakis, "Hybrid simulated annealing-tabu search method for optimal sizing of autonomous power systems with renewables," *IEEE Trans. Sustain. Energy*, vol. 3, no. 3, pp. 330–338, Jul. 2012.
- [23] M. A. Mohamed, A. M. Eltamaly, and A. I. Alolah, "Swarm intelligence-based optimization of grid-dependent hybrid renewable energy systems," *Renew. Sustain. Energy Rev.*, vol. 77, pp. 515–524, Sep. 2017.
- [24] S. Singh, M. Singh, and S. C. Kaushik, "Feasibility study of an islanded microgrid in rural area consisting of PV, wind, biomass and battery energy storage system," *Energy Convers. Manage.*, vol. 128, pp. 178–190, Nov. 2016.
- [25] S. Sanajaoba and E. Fernandez, "Maiden application of Cuckoo search algorithm for optimal sizing of a remote hybrid renewable energy system," *Renew. Energy*, vol. 96, pp. 1–10, Oct. 2016.
- [26] I. Ullah, Z. Khitab, M. Khan, and S. Hussain, "An efficient energy management in office using bio-inspired energy optimization algorithms," *Processes*, vol. 7, no. 3, p. 142, Mar. 2019.
- [27] S. Sanajaoba, "Optimal sizing of off-grid hybrid energy system based on minimum cost of energy and reliability criteria using firefly algorithm," *Sol. Energy*, vol. 188, pp. 655–666, Aug. 2019.
- [28] J.-S. Chou and D.-N. Truong, "A novel Metaheuristic optimizer inspired by behavior of jellyfish in ocean," *Appl. Math. Comput.*, vol. 389, Jan. 2021, Art. no. 125535.
- [29] M. Iqbal, M. Sajjad, S. Amin, S. Haroon, R. Liaqat, M. Khan, M. Waseem, and M. Shah, "Optimal scheduling of residential home appliances by considering energy storage and stochastically modelled photovoltaics in a grid exchange environment using hybrid grey wolf genetic algorithm optimizer," *Appl. Sci.*, vol. 9, no. 23, p. 5226, Dec. 2019.
- [30] M. Z. Gunduz and R. Das, "Cyber-security on smart grid: Threats and potential solutions," *Comput. Netw.*, vol. 169, Mar. 2020, Art. no. 107094, doi: 10.1016/j.comnet.2019.107094.
- [31] K. Anoune, M. Bouya, A. Astito, and A. B. Abdellah, "Sizing methods and optimization techniques for PV-wind based hybrid renewable energy system: A review," *Renew. Sustain. Energy Rev.*, vol. 93, pp. 652–673, Oct. 2018.
- [32] A. M. Eltamaly, M. S. Al-Saud, and A. G. Abokhalil, "A novel bat algorithm strategy for maximum power point tracker of photovoltaic energy systems under dynamic partial shading," *IEEE Access*, vol. 8, pp. 10048–10060, 2020.
- [33] A. M. Eltamaly and A. A. Al-Shamma'a, "Optimal configuration for isolated hybrid renewable energy systems," *J. Renew. Sustain. Energy*, vol. 8, no. 4, 2016, Art. no. 045502.
- [34] A. M. Eltamaly, M. S. Al-Saud, A. G. Abokhalil, and H. M. H. Farh, "Simulation and experimental validation of fast adaptive particle swarm optimization strategy for photovoltaic global peak tracker under dynamic partial shading," *Renew. Sustain. Energy Rev.*, vol. 124, May 2020, Art. no. 109719.
- [35] A. Eltamaly and M. Mohamed, "Optimal sizing and designing of hybrid renewable energy systems in smart grid applications," in *Advances in Renewable Energies and Power Technologies*. Amsterdam, The Netherlands: Elsevier, 2018, pp. 231–313.
- [36] E. Skoplaki, A. G. Boudouvis, and J. A. Palyvos, "A simple correlation for the operating temperature of photovoltaic modules of arbitrary mounting," *Sol. Energy Mater. Sol. Cells*, vol. 92, no. 11, pp. 1393–1402, Nov. 2008.
- [37] A. Kaabeche, M. Belhameel, and R. Ibtouen, "Optimal sizing method for stand-alone hybrid PV/wind power generation system," in *Proc. SMEE*, 2010, pp. 205–213.
- [38] D. Guasch and S. Silvestre, "Dynamic battery model for photovoltaic applications," *Prog. Photovolt., Res. Appl.*, vol. 11, no. 3, pp. 193–206, 2003.
- [39] (2020). *Retail Energy Price Data*. [Online]. Available: <https://www.globalpetrolprices.com/>
- [40] R. Dufo-López and J. L. Bernal-Agustín, "Multi-objective design of PV-wind-diesel-hydrogen-battery systems," *Renew. Energy*, vol. 33, no. 12, pp. 2559–2572, Dec. 2008.
- [41] Raviteja Ganapathinedi. (2021). *Solar PV Wind Hybrid Energy System*. Accessed: Jun. 3, 2021. [Online]. Available: <https://www.mathworks.com/matlabcentral/fileexchange/72764-solar-pv-wind-hybrid-energy-system>
- [42] A. M. Eltamaly, "A novel musical chairs algorithm applied for MPPT of PV systems," *Renew. Sustain. Energy Rev.*, vol. 146, Aug. 2021, Art. no. 111135.
- [43] A. M. Eltamaly, "An improved Cuckoo search algorithm for maximum power point tracking of photovoltaic systems under partial shading conditions," *Energies*, vol. 14, no. 4, p. 953, Feb. 2021.
- [44] A. M. Eltamaly, A. I. Alolah, and M. Y. Abdulghany, "Digital implementation of general purpose fuzzy logic controller for photovoltaic maximum power point tracker," in *Proc. SPEEDAM*, Jun. 2010, pp. 622–627.
- [45] A. M. Eltamaly, "Modeling of wind turbine driving permanent magnet generator with maximum power point tracking system," *J. King Saud Univ.-Eng. Sci.*, vol. 19, no. 2, pp. 223–236, 2007.
- [46] J. C. Oviedo-Cepeda, I. Serna-Suárez, G. Osma-Pinto, C. Duarte, J. Solano, and H. A. Gabbar, "Design of tariff schemes as demand response mechanisms for stand-alone microgrids planning," *Energy*, vol. 211, Nov. 2020, Art. no. 119028.
- [47] Y. Zhang, A. Lundblad, P. E. Campana, F. Benavente, and J. Yan, "Battery sizing and rule-based operation of grid-connected photovoltaic-battery system: A case study in Sweden," *Energy Convers. Manage.*, vol. 133, pp. 249–263, Feb. 2017.
- [48] T. Lühn and J. Geldermann, "Operating strategies for battery storage systems in low-voltage grids to limit the feed-in power of solar power systems using fuzzy control," *Zeitschrift Energiewirtschaft*, vol. 41, no. 3, pp. 169–186, Sep. 2017.
- [49] M. J. Hadidian-Moghaddam, S. Arabi-Nowdeh, and M. Bigdeli, "Optimal sizing of a stand-alone hybrid photovoltaic/wind system using new grey wolf optimizer considering reliability," *J. Renew. Sustain. Energy*, vol. 8, no. 3, May 2016, Art. no. 035903.
- [50] D. Saheb-Koussa, M. Koussa, M. Belhameel, and M. Haddadi, "Economic and environmental analysis for grid-connected hybrid photovoltaic-wind power system in the arid region," *Energy Procedia*, vol. 6, pp. 361–370, Jan. 2011.
- [51] V. O. Okinda and N. O. Abungu, "A review of techniques in optimal sizing of hybrid renewable energy systems," *Int. J. Res. Eng. Technol.*, vol. 4, no. 11, pp. 153–163, Nov. 2015.
- [52] M. A. Mohamed, A. M. Eltamaly, A. I. Alolah, and A. Y. Hatata, "A novel framework-based cuckoo search algorithm for sizing and optimization of grid-independent hybrid renewable energy systems," *Int. J. Green Energy*, vol. 16, no. 1, pp. 86–100, 2019.
- [53] F. Mostofi and H. Shayeghi, "Feasibility and optimal reliable design of renewable hybrid energy system for rural electrification in Iran," *Int. J. Renew. Energy Res.*, vol. 2, no. 4, pp. 574–582, 2012.
- [54] X. S. Yang and S. Deb, "Cuckoo search via Lévy flights," in *Proc. IEEE Nature Biologically Inspired Comput. (NaBIC)*, Coimbatore, India, Dec. 2009, pp. 210–214.
- [55] N. Hashim and Z. Salam, "Critical evaluation of soft computing methods for maximum power point tracking algorithms of photovoltaic systems," *Int. J. Power Electron. Drive Syst.*, vol. 10, no. 1, p. 548, Mar. 2019.
- [56] A. M. Eltamaly, "A novel strategy for optimal PSO control parameters determination for PV energy systems," *Sustainability*, vol. 13, no. 2, p. 1008, Jan. 2021.
- [57] *AE-Italia STOMA ST-K60/D21*. [Online]. Available: <https://en.wind-turbine-models.com/turbines/1026-ae-italia-stoma-st-k60-d21>

- [58] A. Maleki, F. Pourfayaz, and M. A. Rosen, "A novel framework for optimal design of hybrid renewable energy-based autonomous energy systems: A case study for Namin, Iran," *Energy*, vol. 98, pp. 168–180, Mar. 2016.
- [59] S. Jamshidi, K. Pourhossein, and M. Asadi, "Size estimation of wind/solar hybrid renewable energy systems without detailed wind and irradiation data: A feasibility study," *Energy Convers. Manage.*, vol. 234, Apr. 2021, Art. no. 113905.
- [60] M. Gharibi and A. Askarzadeh, "Size and power exchange optimization of a grid-connected diesel generator-photovoltaic-fuel cell hybrid energy system considering reliability, cost and renewability," *Int. J. Hydrogen Energy*, vol. 44, no. 47, pp. 25428–25441, Oct. 2019.
- [61] A. Aziz, M. Tajuddin, M. Adzman, M. Ramli, and S. Mekhilef, "Energy management and optimization of a PV/diesel/battery hybrid energy system using a combined dispatch strategy," *Sustainability*, vol. 11, no. 3, p. 683, Jan. 2019.
- [62] Y. Khawaja, D. Giaouris, H. Patsios, and M. Dahidah, "Optimal cost-based model for sizing grid-connected PV and battery energy system," in *Proc. IEEE Jordan Conf. Appl. Electr. Eng. Comput. Technol. (AEECT)*, Oct. 2017, pp. 1–6.
- [63] X. Luo, J. Wang, M. Dooner, and J. Clarke, "Overview of current development in electrical energy storage technologies and the application potential in power system operation," *Appl. Energy*, vol. 137, pp. 511–536, Jan. 2015.
- [64] C. Ju, P. Wang, L. Goel, and Y. Xu, "A two-layer energy management system for microgrids with hybrid energy storage considering degradation costs," *IEEE Trans. Smart Grid*, vol. 9, no. 6, pp. 6047–6057, Nov. 2018.



ALI M. ELTAMALY received the B.Sc. and M.Sc. degrees in electrical engineering from Al-Minia University, Egypt, in 1992 and 1996, respectively, and the Ph.D. degree in electrical engineering from Texas A&M University, in 2000. He is currently a Full Professor with King Saud University, Saudi Arabia, and Mansoura University, Egypt. He has published 15 books and book chapters. He has authored or coauthored more than 200 refereed journal articles and conference papers, and a number of patents with the U.S. Patent Office. He has supervised several M.Sc. and Ph.D. theses, and worked on number of technical projects.

His current research interests include renewable energy, smart grids, power electronics, motor drives, power quality, artificial intelligence, evolutionary and heuristic optimization techniques, and distributed generation. He received the Professor Award for Scientific Excellence from the Egyptian Supreme Council of Universities, Egypt, in June 2017, and has been awarded many prizes from different universities in Egypt and Saudi Arabia. He has chaired many international conference sessions. He participates as an editor and an associate editor for many international journals.



MAJED A. ALOTAIBI (Member, IEEE) received the B.Sc. degree in electrical engineering from King Saud University, Riyadh, Saudi Arabia, in 2010, and the M.A.Sc. and Ph.D. degrees in electrical and computer engineering from the University of Waterloo, Waterloo, Canada, in 2014 and 2018, respectively. He worked as an Electrical Design Engineer with ABB Saudi Arabia. He is currently an Assistant Professor with the Department of Electrical Engineering, King Saud University. His research interests include power system planning, operation, renewable energy modeling, applied optimization, and smart grid. He served as a Reviewer for IEEE TRANSACTIONS ON POWER SYSTEMS and IEEE TRANSACTIONS ON SMART GRID.

• • •